

Copyright

by

Yang Du

2014

**The Thesis Committee for Yang Du
Certifies that this is the approved version of the following thesis:**

**Thermodynamics of Aqueous Piperazine/Aminoethylpiperazine for CO₂
Capture**

**APPROVED BY
SUPERVISING COMMITTEE:**

Supervisor:

Gary T. Rochelle

Thomas F. Edgar

**Thermodynamics of Aqueous Piperazine/Aminoethylpiperazine for CO₂
Capture**

by

Yang Du, B.S.; M.S.

Thesis

Presented to the Faculty of the Graduate School of

The University of Texas at Austin

in Partial Fulfillment

of the Requirements

for the Degree of

Master of Science in Engineering

The University of Texas at Austin

May 2014

Dedication

To my family

Abstract

Thermodynamics of Aqueous Piperazine/Aminoethylpiperazine for CO₂ Capture

Yang Du, M.S.E

The University of Texas at Austin, 2014

Supervisor: Gary T. Rochelle

Aqueous piperazine (PZ) blended with N-(2-aminoethyl) piperazine (AEP) is an attractive solvent for CO₂ capture from coal-fired power plants. Blending PZ with AEP can remediate the precipitation issue of concentrated PZ while maintaining its high CO₂ absorption rate, and high resistance to degradation. 5 m PZ/2 m AEP also shows a milder nitrosamine issue than concentrated piperazine. A rigorous thermodynamic model was developed in Aspen Plus[®] to predict properties of PZ/AEP/H₂O/CO₂, using the electrolyte-Nonrandom Two-Liquid (eNRTL) activity coefficient model. A sequential regression was performed to represent CO₂ solubility, speciation, and amine volatility data over operationally significant loading and temperature ranges. The model predicts a CO₂ cyclic capacity of 0.78 mol/kg (PZ + AEP + water) for 5 m PZ/2 m AEP, compared to 0.50 mol/kg for 7 m MEA and 0.86 mol/kg for 8 m PZ. The predicted heat of absorption is 75 to 80 kJ/mol CO₂ at the operating loading range (0.290–0.371 mol CO₂/mol alkalinity). Although 5 m PZ/2 m AEP has a slightly lower CO₂ capacity than 8 m piperazine, its higher heat of absorption may offset the negative effect on energy

consumption. Speciation for PZ/AEP/H₂O at various CO₂ loading and temperature was also predicted, from which behavior of CO₂ in the amine system was proposed.

Table of Contents

List of Tables	ix
List of Figures	xi
Chapter 1: Introduction	1
1.1 Background and Motivation	1
1.2 Scope of Work	2
Chapter 2: Materials and Methods.....	3
2.1 Solution Preparation.....	3
2.2 Solvent Solubility.....	3
2.3 Viscosity Measurements	3
2.4 Thermal Degradation	4
2.5 Oxidative Degradation.....	4
2.6 Nitrosamine Formation and Decomposition	5
2.7 CO ₂ Absorption Rate and Solubility.....	5
2.8 High Temperature Vapor-liquid Equilibrium	5
2.9 Quantitative NMR Measurement.....	6
Chapter 3: Characterization of PZ/AEP as a solvent for CO ₂ capture.....	7
3.1 Solid Solubility of PZ/AEP.....	7
3.2 Viscosity	8
3.3 Thermal Degradation	9
3.3.1 Thermal degradation kinetics.....	9
3.3.2 The effect of CO ₂	11
3.3.3 Thermal degradation products	12
3.3.4 Proposed thermal degradation pathways of PZ/AEP.....	18
3.4 Oxidative Degradation.....	20
3.5 Nitrosamines	21
3.6 CO ₂ Solubility.....	23
3.7 Absorption rate.....	25

Chapter 4: Thermodynamic modeling of PZ/AEP.....	27
4.1 Thermodynamic Framework.....	27
4.1.1 Aqueous-phase chemical equilibrium.....	27
4.1.2 Reference state and units	30
4.1.3 Reaction equilibrium.....	31
4.1.4 Vapor-liquid phase equilibrium	35
4.1.5 Vapor phase behavior	36
4.1.6 System non-idealities.....	36
4.2 Results and Discussion	39
4.2.1 Identification of ^{13}C NMR spectra.....	39
4.2.2 AEP-H ₂ O.....	40
4.2.3 AEP-H ₂ O-CO ₂	42
4.2.4 PZ/AEP/H ₂ O/CO ₂	46
4.2.5 Heat of absorption prediction.....	51
Chapter 5: Conclusions	54
Appendix A: Tabulated Experimental Data.....	56
References.....	63

List of Tables

Table 3.1:	Viscosity of 5 m PZ/2 m AEP from 20 to 60 °C.	9
Table 3.2:	Apparent first order rate constant (k_1) for thermal degradation of PZ/AEP and other related solvents (Freeman 2011).....	10
Table 3.3:	Summary of capacity, absorption rate, heat of absorption, and maximum stripper temperature for 5 m PZ/ 2 m AEP and other conventional amines (Li et al., 2013).	26
Table 4.1:	Molecular structure of the compounds in CO ₂ -loaded PZ-AEP aqueous solutions.	28
Table 4.2:	Summary of model parameters.	38
Table 4.3:	Regressed parameters and standard error for AEP/H ₂ O regression..	41
Table 4.4:	The adjusted parameters for 6 m AEP-CO ₂ -H ₂ O	46
Table 4.5:	Regressed parameters and standard error.	48
Table 4.6:	Summary of non-adjusted and non-temperature dependence parameters used in this model.	49
Table 4.7:	Summary of non-adjusted and temperature dependence parameters used in this model.....	49
Table A. 1:	Transition temperatures for PZ/AEP blend.....	56
Table A. 2:	Tabulated Experimental Data for thermal degradation of 5 m PZ/2 m AEP (0.3 mole CO ₂ per mole alkalinity initially, 175 °)	57
Table A. 3:	Tabulated Experimental Data for oxidation of 2 m AEP at 70 °C in the presence of 0.1 mM Mn ²⁺ and with the typical SSM mixture (0.4 mM Fe ²⁺ , 0.05 mM Cr ³⁺ and 0.1 mM Ni ²⁺).....	58

Table A. 4: Tabulated Experimental Data for oxidation of 8 m PZ at 70 °C in the presence of 0.1 mM Mn ²⁺ and with the typical SSM mixture (0.4 mM Fe ²⁺ , 0.05 mM Cr ³⁺ and 0.1 mM Ni ²⁺).....	59
Table A. 5: Tabulated Experimental Data for formation of nitrosamines in 5 m PZ/2 m AEP and 2 m AEP at 0.3 mol CO ₂ /mol alkalinity and 100 °C	60
Table A. 6: Tabulated Experimental Data for nitrosamine decomposition in 5 m PZ/2 m AEP and 2 m AEP at 0.3 mol CO ₂ /mol alkalinity and 150 °C	61
Table A. 7: Tabulated Experimental Data for CO ₂ solubility in 5 m PZ/2 m AEP at high temperature	62

List of Figures

- Figure 3.1: Liquid-Solid transition temperature for PZ/AEP with different amine ratios, ●: 8 m PZ/0 m AEP (Freeman 2011); ■: 5 m PZ/2 m AEP; ◆: 4 m PZ/2.67 m AEP; ▲: 3 m PZ/3.33 m AEP.8
- Figure 3.2: Comparison of PZ loss in 5 m PZ/2 m AEP and 8 m pure PZ (Freeman and Rochelle 2011) in thermal degradation at 0.3 mol CO₂/mol alkalinity.10
- Figure 3.3: Comparison of AEP loss in 5 m PZ/2 m AEP and 5.33 m AEP with thermal degradation at 0.3 mol CO₂/mol alkalinity.11
- Figure 3.4: Effect of CO₂ on the degradation of PZ and AEP in 5 m PZ/2 m AEP at 175 °C (Dashed line: 0.2 mol CO₂/mol alkalinity; solid line: 0.3 mol CO₂/mol alkalinity).12
- Figure 3.5: Cation IC chromatogram of the initial and final sample of 5 m PZ/2 m AEP at 175 °C (U: unknown).13
- Figure 3.6: Mass spectrum for PZ/AEP degradation at 150°C for 5 weeks.14
- Figure 3.7: Production of carboxylate ions during thermal degradation of 5 m PZ/2 m AEP at 175°C.....16
- Figure 3.8: Degradation products from thermal degradation of 5 m PZ/2 m AEP with 0.3 mol CO₂/mol alkalinity at 175 °C.....17
- Figure 3.9: PZ, AEP, and CO₂ loss and generation of major degradation products for 5 m PZ/2 m AEP with 0.3 mol CO₂/mol alkalinity at 175 °C.18
- Figure 3.10: Comparison of total formate production in 5 m PZ/2 m AEP, 8 m PZ with Mn²⁺, 8 m PZ without Mn²⁺ (Sexton and Rochelle, 2009), 2 m AEP and 7 m MEA (Sexton and Rochelle, 2009) at 70 °C.....21

Figure 3.11: Nitrosamine formation in 5 m PZ/2 m AEP at 100 °C, compared to that in 8 m PZ (Fine et al., 2013) and 2 m AEP (the initial nitrite concentration was 40 mmol/kg solvent for all the three solvents)....	22
Figure 3.12: Nitrosamine decomposition in 5 m PZ/2 m AEP at 150 °C, compared to that in 8 m PZ (Fine et al., 2013) and 2 m AEP.....	23
Figure 3.13: CO ₂ solubility for 5 m PZ/2 m AEP (Solid lines: 5 m PZ/2 m AEP equation model; Solid circles: measured data for 5 m PZ/2 m AEP using WWC; Open circles: measured data for 5 m PZ/2 m AEP using SA; Dashed lines: 8 m PZ equation model from Xu (2011))......	24
Figure 3.14: Mass transfer coefficients (kg [']) in 5 m PZ/2 m AEP (solid lines) from 20 to 80 °C, compared to that in 8 m PZ (dashed line) at 40 °C.	26
Figure 4.1: ¹³ C NMR spectra for 6 m AEP (a) and 5 m PZ/2 m AEP (b) at 25 °C and CO ₂ loading of 0.3.....	40
Figure 4.2: AEP vapor pressure predicted by the model compared with experimental data, as well as data for 8 m PZ with no CO ₂ loading (Nguyen et al., 2011). Filled Points: Experimental data; Solid lines: Model prediction from this work.....	41
Figure 4.3: Experimental measurement (points) (Chen and Rochelle 2011) and Aspen Plus [®] predictions (lines) for VLE of loaded 6 m AEP solution between 20 °C and 160 °C.....	43
Figure 4.4: ¹³ C speciation for 6 m AEP-CO ₂ -H ₂ O at 25 °C.....	44
Figure 4.5: Predicted speciation distribution for 6 m AEP-CO ₂ -H ₂ O at 40 °C...	45
Figure 4.6: Comparison of Aspen Plus [®] predictions (lines) and experimental data (points) for loaded 5 m PZ/2 m AEP between 20 °C and 160 °C.....	48
Figure 4.7: Speciation validation for 5 m PZ/2 m AEP.	50

Figure 4.8: Predicted speciation distribution for 6 m AEP-CO ₂ -H ₂ O at 40 °C...	51
Figure 4.9: Aspen Plus® model predictions of heat of absorption for 6 m AEP using Lewis and Randall Equation (points) and calorimetric (lines) calculations.	52
Figure 4.10: Aspen Plus® model predictions of heat of absorption for 5 m PZ/2 m AEP using Lewis and Randall Equation (points) and calorimetric (lines) calculations.	53

Chapter 1: Introduction

1.1 BACKGROUND AND MOTIVATION

Amine scrubbing has shown the most promise for effective capture of CO₂ from coal-fired flue gas (Rochelle 2009). Aqueous monoethanolamine (MEA) with a concentration between 15 – 30 wt % has been previously used in similar applications such as CO₂ removal from natural gas and hydrogen, and is currently considered the state-of-the-art technology for CO₂ absorption/stripping because of its effectiveness for CO₂ capture and low cost of production. However, the low resistance to degradation, and moderate CO₂ capacity and CO₂ absorption rates of MEA lead to a significant energy penalty and capital cost for CO₂ capture from coal-fired flue gas.

Concentrated piperazine (PZ) has been proposed as a possible alternative to 30 wt % MEA (Rochelle et al., 2011). PZ has about twice the CO₂ absorption rate and CO₂ capacity, and greater resistance to oxidative and thermal degradation than 30 wt % MEA, which can lower the heat duty for the stripper in amine scrubbing systems by approximately 10% (Rochelle et al., 2011).

In spite of desirable characteristics, the application of concentrated PZ in industry may be limited by solid precipitation at both lean and rich CO₂ loading (Rochelle et al., 2011). At room temperature (20 °C), 8 m PZ requires a loading of 0.26 mol CO₂/mol alkalinity to stay in solution and also forms solids at high CO₂ loading.

Blending solvents already in use is one approach to combine desirable characteristics. A novel PZ-based blend, piperazine/N-(2-aminoethyl) piperazine (PZ/AEP), was investigated in this study to remediate the precipitation of concentrated PZ without sacrificing its CO₂ capacity and absorption rate, resistance to degradation, and other desirable characteristics.

To predict the overall performance of this amine blend, it is necessary to develop a rigorous thermodynamic model which can accurately predict the thermodynamic properties, specifically vapor-liquid equilibrium (VLE), calorimetric properties, and chemical reaction equilibrium in process simulation tools.

The thermodynamic properties of a variety of aqueous amine solutions for CO₂ absorption have been successfully modeled with the electrolyte-Nonrandom Two-Liquid (eNRTL) model as a thermodynamic framework. Austgen (1989) used the eNRTL model developed by Chen and coworkers (2001) to model the VLE of carbon dioxide over aqueous N-methyl-diethanolamine (MDEA), monoethanolamine (MEA), diethanolamine (DEA), and Diglycolamine[®] (DGA[®]). Posey (1997) improved Austgen's models by studying the activity coefficient of the amines at infinite dilution. An activity-based PZ-H₂O-CO₂ model was developed by Hilliard (2008) in Aspen Plus[®]. Frailie (2011) extended Hilliard's model to represent various thermodynamic properties of more concentrated PZ solutions and identified this model as the Independence model.

1.2 SCOPE OF WORK

The scope of this research included characterization of PZ/AEP as a solvent for CO₂ capture. Solvent solubility, CO₂ solubility, CO₂ absorption rate, degradation, volatility and nitrosamine formation of this solvent were investigated under various conditions. The data collected from these experiments were used to develop a rigorous thermodynamic model for PZ-AEP-H₂O-CO₂ system in Aspen Plus[®] using eNRTL model as the thermodynamic framework.

Chapter 2: Materials and Methods

2.1 SOLUTION PREPARATION

Aqueous PZ/AEP was prepared by melting anhydrous PZ (99%, Alfa Aesar, Ward Hill, MA) in water and AEP (99%, Alfa Aesar, Ward Hill, MA) mixture, and gravimetrically sparging CO₂ (99.5%, Matheson Tri Gas, Basking Ridge, NJ) to achieve the desired CO₂ concentration. The concentration of CO₂ was determined by total inorganic carbon (TIC) analysis, described by Hilliard (2008).

2.2 SOLVENT SOLUBILITY

The solid solubility of PZ/AEP with a total alkalinity of 16 m was measured in a water bath over a range of PZ/AEP molar ratio (5/2, 4/2.67, 3/3.33), CO₂ loading (from 0 to 0.4 mol CO₂/mol alkalinity), and temperature (from 0 to 50 °C). The solid solubility measurements were based on visual observations and the method was described in detail by Freeman (2011). Solutions with desired properties were heated up to 50 °C in a water bath to melt precipitates in solution with lean CO₂ loading. While cooling slowly, the temperature at which the solution first began to crystallize or precipitate was regarded as the crystallizing transition temperature. Finally, the solution was heated again to carefully observe the temperature when the crystals fully melt and this was noted as the melting transition temperature. The difference between crystallizing and melting transition temperature, which is also called hysteresis, was minimized to 1 °C or less for most of the measured points by giving enough equilibrium time and repeating the melting-crystallizing process at transition temperatures.

2.3 VISCOSITY MEASUREMENTS

Viscosity of 5 m PZ/2 m AEP was measured using a Physica MCR 300 cone and plate rheometer (Anton Paar GmbH, Graz, Austria). The method was also described by

Freeman (2011). The average value and standard deviation calculated from 10 individual measurements for each sample was reported.

2.4 THERMAL DEGRADATION

Thermal degradation was measured in ½-inch OD 316 stainless steel thermal cylinders. Cylinders were filled with 7 mL of amine solution with around 3 mL of headspace, sealed with two Swagelok® end caps, and placed in forced convection ovens maintained at the target temperature. Individual cylinders were removed from the ovens at each sampling point and then analyzed for degradation products, degradation rate, and CO₂ loading, using a Dionex ICS-2500 cation ion chromatograph, a Dionex ICS-3000 modular Dual Reagent-Free anion ion chromatograph (Dionex Corporation) and an infrared CO₂ analyzer (Horiba Instruments Inc., Spring, TX). The details of the experimental apparatus, procedure, and analytical methods were described by Freeman (2011).

2.5 OXIDATIVE DEGRADATION

Oxidative degradation experiments for 8 m PZ and 2 m AEP spiked with 0.05 mM Cr³⁺, 0.1 mM Ni²⁺, 0.4 mM Fe²⁺ and 0.1 mM Mn²⁺ were conducted in a low gas flow agitated reactor with 100 mL/min of a saturated 98%/2% O₂/CO₂ gas mixture fed into the reactor headspace. The duration of the experiment was 2 weeks and 3 ml samples were taken every two to three days and water was added periodically to maintain the water balance of the reactor contents. The liquid samples were analyzed for PZ, AEP, and degradation products using ion chromatography. The details of the experimental apparatus, procedure, and analytical methods were described by Sexton (2009).

2.6 NITROSAMINE FORMATION AND DECOMPOSITION

Nitrosamine formation and decomposition experiments were conducted in $\frac{3}{8}$ -inch Swagelok thermal cylinders using a similar method to thermal degradation experiments. 5 m PZ/2 m AEP or 2 m AEP solutions with 0.3 mol CO₂/mol alkalinity were prepared and spiked gravimetrically with 40 mmol/kg of sodium nitrite (NaNO₂) immediately before being placed into convection ovens at 100 °C and 150 °C. The details of the experimental apparatus, procedure, and analytical methods were described by Fine (2013).

2.7 CO₂ ABSORPTION RATE AND SOLUBILITY

CO₂ absorption rate and equilibrium partial pressure in 5 m PZ/2 m AEP were measured from 20 to 100 °C using a wetted wall column (WWC), which countercurrently contacted an aqueous 5 m PZ/2 m AEP solution with a saturated N₂/CO₂ stream on the surface of a stainless steel rod with a known surface area to simulate the situation of CO₂ absorption in a absorber. The detailed description of wetted wall column measurement was given by Li (2013).

2.8 HIGH TEMPERATURE VAPOR-LIQUID EQUILIBRIUM

The total pressure of 5 m PZ/2 m AEP loaded with CO₂ was measured from 100 to 160 °C using a sealed autoclave (SA). The partial pressure of CO₂ was calculated by subtracting the partial pressure of N₂ and water from the measured total pressure. The pressure of water was assumed to follow Raoult's Law and the pressure of amine was neglected. The experimental method and calculation of CO₂ partial pressure were described in detail by Xu (2011).

2.9 QUANTITATIVE NMR MEASUREMENT

H-NMR and ^{13}C -NMR measurements were conducted for loaded 6 m AEP and 5 m PZ/2 m AEP. All solutions were prepared gravimetrically from ultra-pure deionized water. Amine solutions were loaded with CO_2 by slowly sparging ^{13}C CO_2 . Experimental apparatus, procedure, and analytical methods were described in detail by Hilliard (2008).

Chapter 3: Characterization of PZ/AEP as a solvent for CO₂ capture

This chapter presents the experimental results for PZ/AEP, including solvent solubility, CO₂ solubility, CO₂ absorption rate, degradation, volatility and nitrosamine formation of this solvent under various conditions.

3.1 SOLID SOLUBILITY OF PZ/AEP

The melting transition temperature of PZ/AEP with variable amine concentration ratio (5/2, 4/2.67, 3/3.33) over a range of CO₂ loading from 0 to 0.4 mol/mol alkalinity is shown in Figure 3.1. The transition temperature for non-blended 8 m PZ from Freeman (2011) is also shown in Figure 3.1 for comparison. As the proportion of PZ in the blend decreases, the transition temperature decreases. For 5 m PZ/2 m AEP, a CO₂ loading of approximately 0.22 mol/mol alkalinity is required to maintain a liquid solution without precipitation at room temperature (20 °C), which is lower than 0.26 mol/mol alkalinity required for 8 m PZ. Unlike 8 m PZ, which also precipitates when CO₂ loading reaches 0.44 mol CO₂/mol alkalinity, no precipitate was observed for the three blends at rich CO₂ loading (until CO₂ reached its solubility limit under atmospheric pressure, which is about 0.4 mol CO₂/mol alkalinity for the three blends). Therefore, 5 m PZ/2 m AEP has a lower solvent solubility limit at lean loading, and is free from precipitation at rich loading under atmospheric pressure.

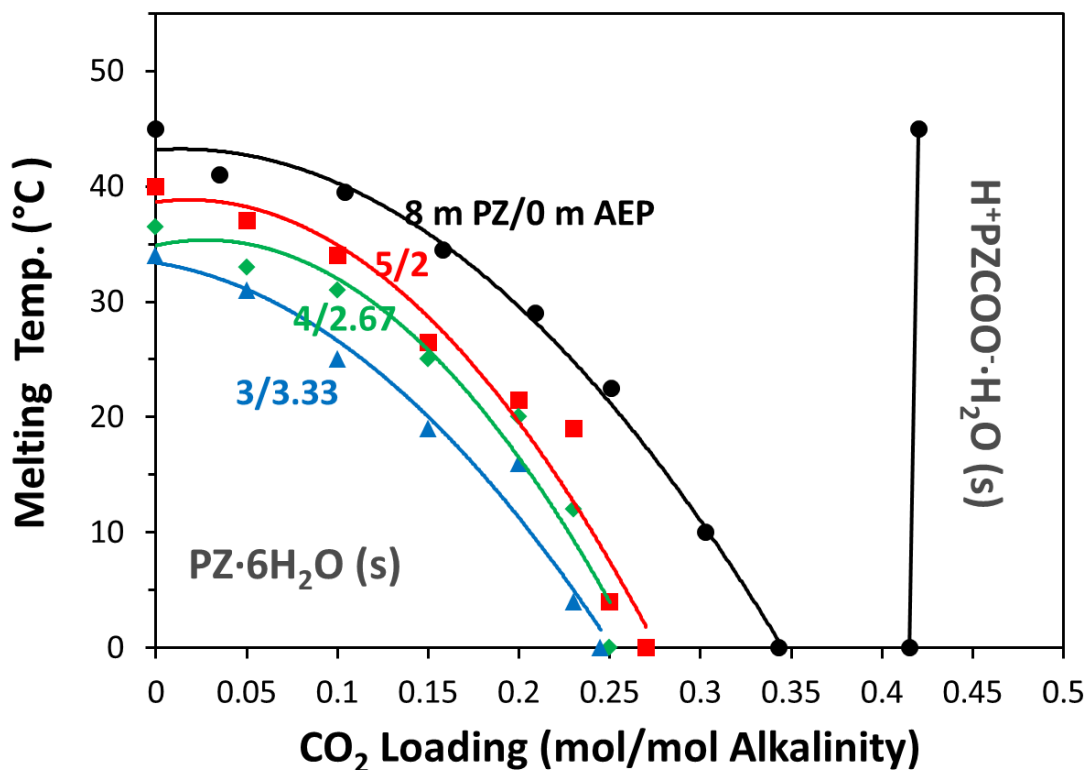


Figure 3.1: Liquid-Solid transition temperature for PZ/AEP with different amine ratios, ●: 8 m PZ/0 m AEP (Freeman 2011); ■: 5 m PZ/2 m AEP; ◆: 4 m PZ/2.67 m AEP; ▲: 3 m PZ/3.33 m AEP.

3.2 VISCOSITY

Viscosity of 5 m PZ/2 m AEP with 0.2 and 0.3 mol CO₂/mol alkalinity was measured at 20 °C, 40 °C, and 60 °C (Table 3.1). The results suggests that the viscosity of this blend is comparable to that of non-blended 8 m PZ (Freeman et al., 2009) (i.e., 11.96 cP for 5 m PZ/2 m AEP compared to 9.99 cP for 8 m PZ at 0.30 mol CO₂/mol alkalinity and 40 °C). The data also demonstrate the expected trend that viscosity increases with increasing CO₂ concentration and decreasing temperature.

Table 3.1: Viscosity of 5 m PZ/2 m AEP from 20 to 60 °C.

CO ₂ Loading (mol/mol alkalinity)	Viscosity (cP)		
	20 °C	40 °C	60 °C
0.20	21.92 ± 0.07	9.84 ± 0.08	5.88 ± 0.16
0.30	24.75 ± 0.09	11.96 ± 0.11	7.78 ± 0.72

3.3 THERMAL DEGRADATION

3.3.1 Thermal degradation kinetics

The thermal degradation of 5 m PZ/2 m AEP was measured for 20 weeks with 0.3 mol CO₂/mol alkalinity at 150 °C and 175 °C. After the 20-week experiment, the loss of PZ and AEP at 150 °C was approximately 10% and 30%, respectively, while at 175 °C the amines were almost entirely degraded (Figures 3.2 and 3.3). The degradation process at 150 °C and 175 °C was well characterized by first order kinetic models. From these results it can be concluded that 5 m PZ/2 m AEP is thermally stable up to 150 °C but not 175 °C.

The thermal degradation of 5 m PZ/2 m AEP is compared to that of 5.33 m non-blended AEP and 8 m PZ (Freeman 2011) (Figures 3.2 and 3.3), and their apparent first order rate constants (k_1) for thermal degradation is given in Table 3.2, along with the data for 7 m MEA. The PZ in this blend degrades at the same rate as in 8 m PZ at both temperatures (Figure 3.2). However, the AEP in the blend degraded much more slowly than in 5.33 m AEP with 0.3 mol CO₂/mol alkalinity (Figure 3.3). This could have two explanations: 1) compared to 2 m AEP, due to the competition of PZ for H⁺, this blend produced less protonated AEP, which is likely to be the initiating species required for the initial reactions of thermal degradation (Freeman and Rochelle 2011); 2) as PZ is one of the major products for AEP thermal degradation, its presence may inhibit the degradation of AEP. The overall amine degradation rate of this blend is on the same scale as that of 8 m PZ, while much smaller than that of 5.33 m AEP and 7 m MEA.

Table 3.2: Apparent first order rate constant (k_1) for thermal degradation of PZ/AEP and other related solvents (Freeman 2011).

Amine	Components	Loading mol/mol alkalinity	$k_1 \times 10^{-9} \text{ (s}^{-1}\text{)}$	
			150 °C	175 °C
PZ	5 m PZ/2 m AEP	0.3	10.2	162
AEP	5 m PZ/2 m AEP	0.3	27.9	388
PZ/AEP	5 m PZ/2 m AEP	0.3	15.2	201
PZ	8 m PZ	0.3	6.1	140
AEP	5.33 m AEP	0.3	365	2022
MEA	7 m MEA	0.4	807	N/A

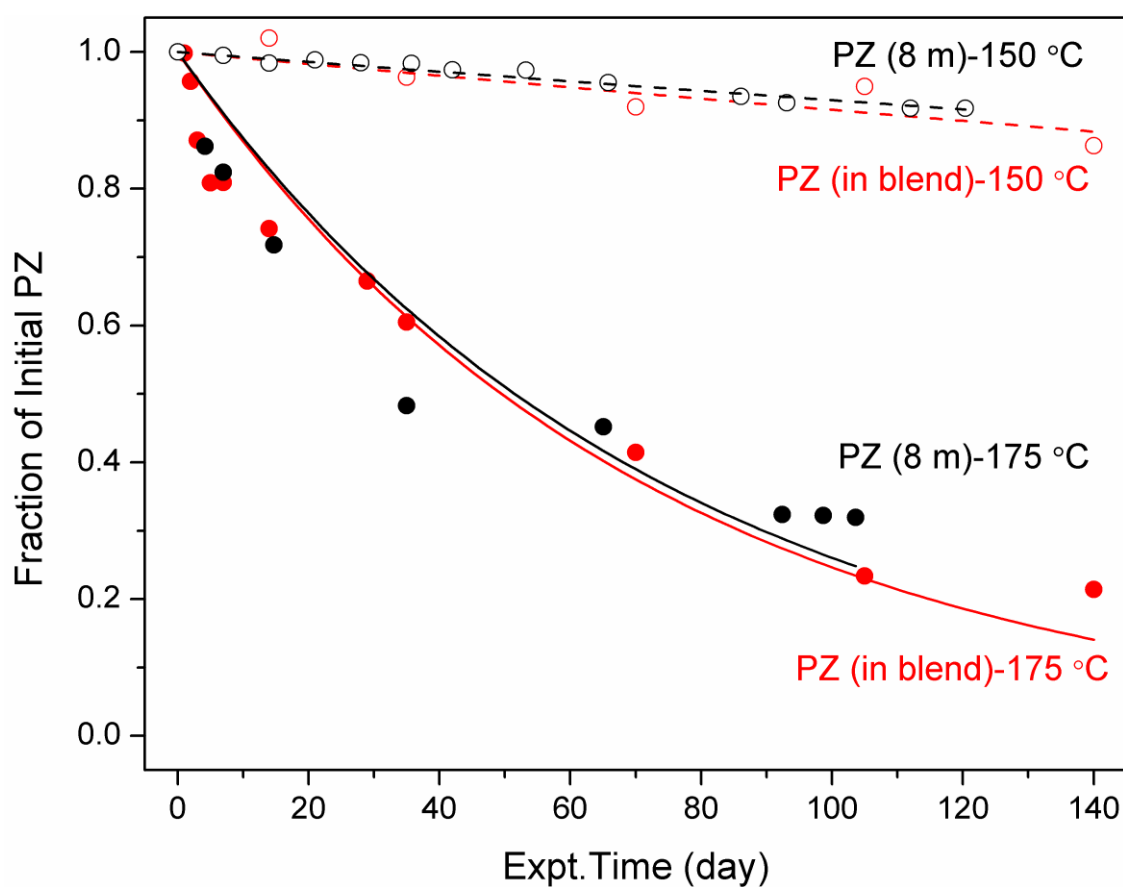


Figure 3.2: Comparison of PZ loss in 5 m PZ/2 m AEP and 8 m pure PZ (Freeman and Rochelle, 2011) in thermal degradation at 0.3 mol CO₂/mol alkalinity.

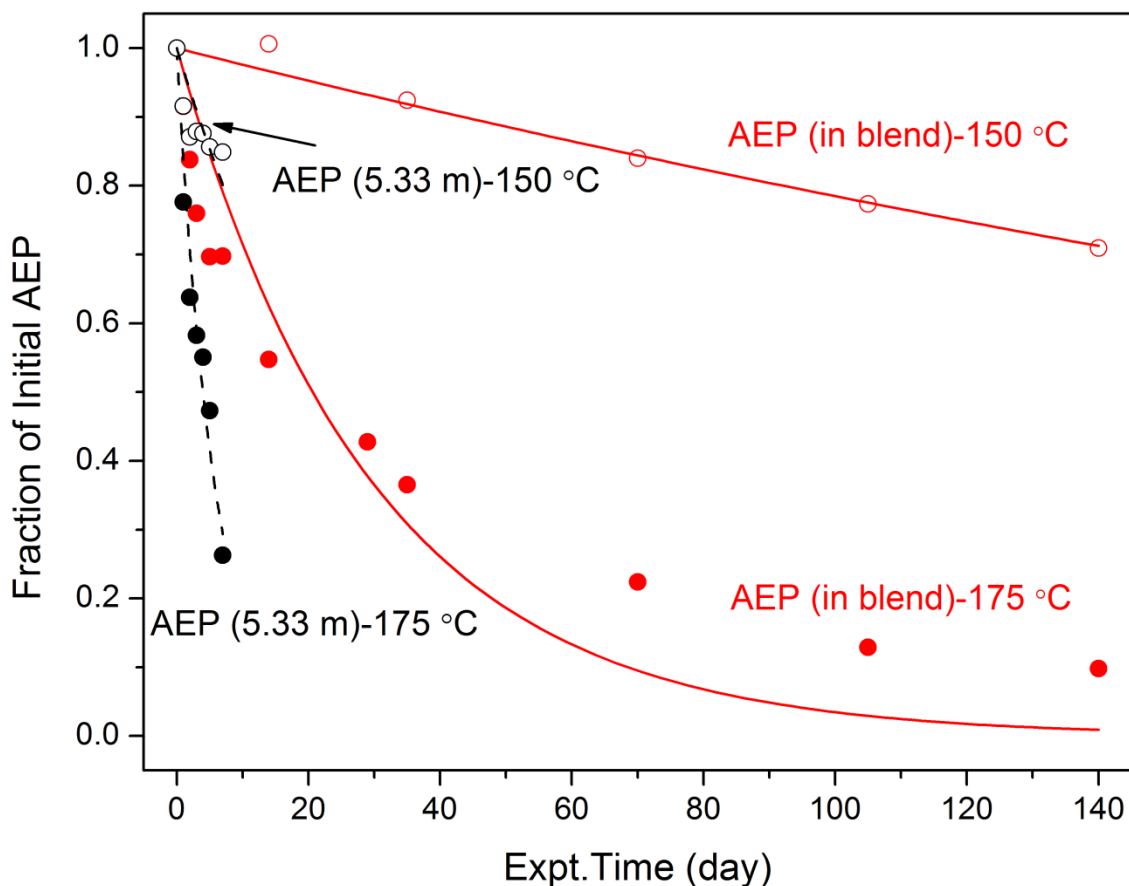


Figure 3.3: Comparison of AEP loss in 5 m PZ/2 m AEP and 5.33 m AEP with thermal degradation at 0.3 mol CO₂/mol alkalinity.

3.3.2 The effect of CO₂

The effect of CO₂ on the degradation of PZ and AEP in 5 m PZ/2 m AEP at 175 °C is given in Figure 3.4. The increase of CO₂ accelerated the degradation of both PZ and AEP in this blend. This can be ascribed to the increased protonated PZ/AEP species present in solution, which are likely to be the initiating species required for the initial reactions of thermal degradation (Freeman and Rochelle, 2011).

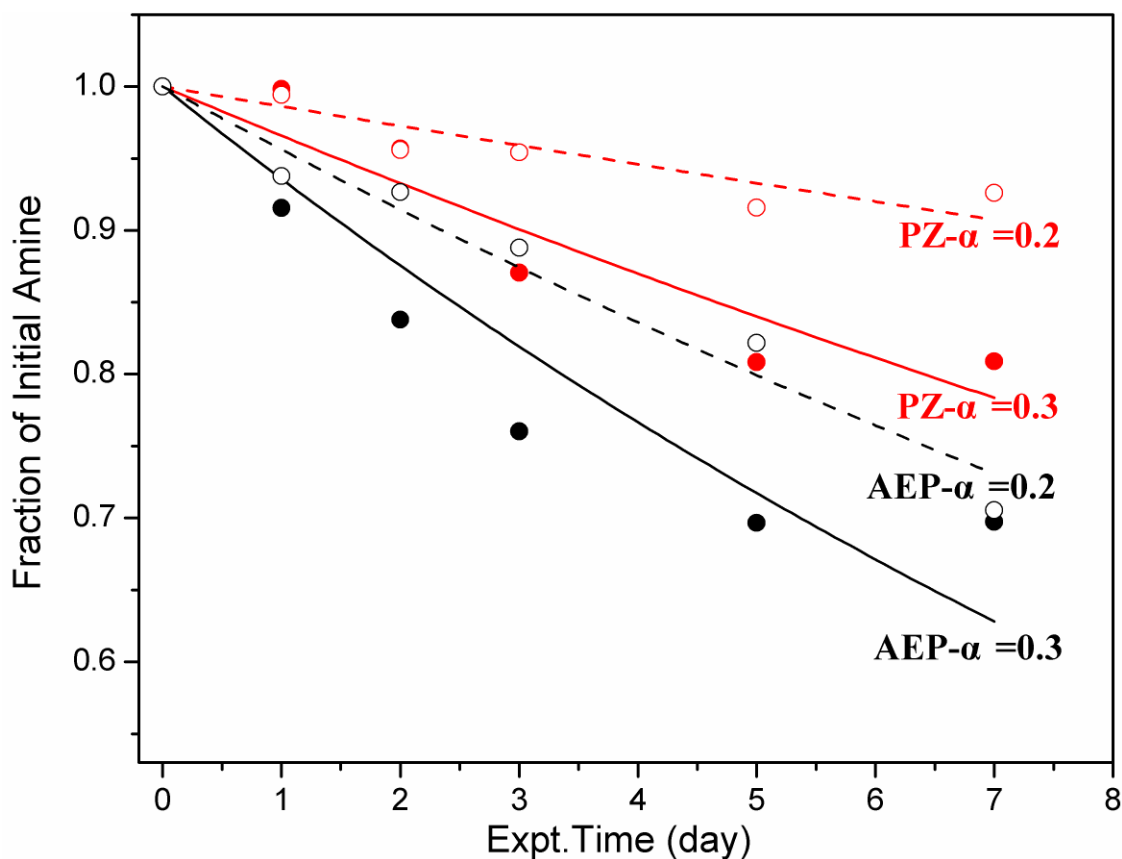


Figure 3.4: Effect of CO₂ on the degradation of PZ and AEP in 5 m PZ/2 m AEP at 175 °C (Dashed line: 0.2 mol CO₂/mol alkalinity; solid line: 0.3 mol CO₂/mol alkalinity).

3.3.3 Thermal degradation products

Degradation products of 5 m PZ/2 m AEP were identified using cation and anion chromatography and mass spectrometry. The loss of CO₂ during degradation was measured by TIC. The cation chromatogram for the sample after 5 weeks of thermal degradation is shown in Figure 3.5. NH₄⁺, N-Formyl PZ (FPZ), PZ, 1-Ethyl PZ (EPZ), Triethylenediamine (TEDA) and AEP peaks were identified using their standards. The remaining peaks shown on the cation chromatogram were identified based on the analysis of PZ thermal degradation products by Freeman (2011) using IC-MS, GC-MS and High Resolution GC-MS (HRGC). The presence of 1-[2-[(2-aminoethyl)amino]ethyl] PZ

(AEAEPZ) / N,N'-di(2-aminoethyl) piperazine (DAEP) (m/z 172.9) and AEAEPZ urea / 1,1'-(1,2-ethanediyl)bis-PZ (PEP) (m/z 199.0) were verified using mass spectroscopy on the sample of PZ/AEP held at 150°C for 5 weeks (Figure 3.6). There were 2 major peaks of products at retention times of 17.7 and 47.6 minutes that have yet to be positively identified and quantified. The degradation products are listed in Table 3.3.

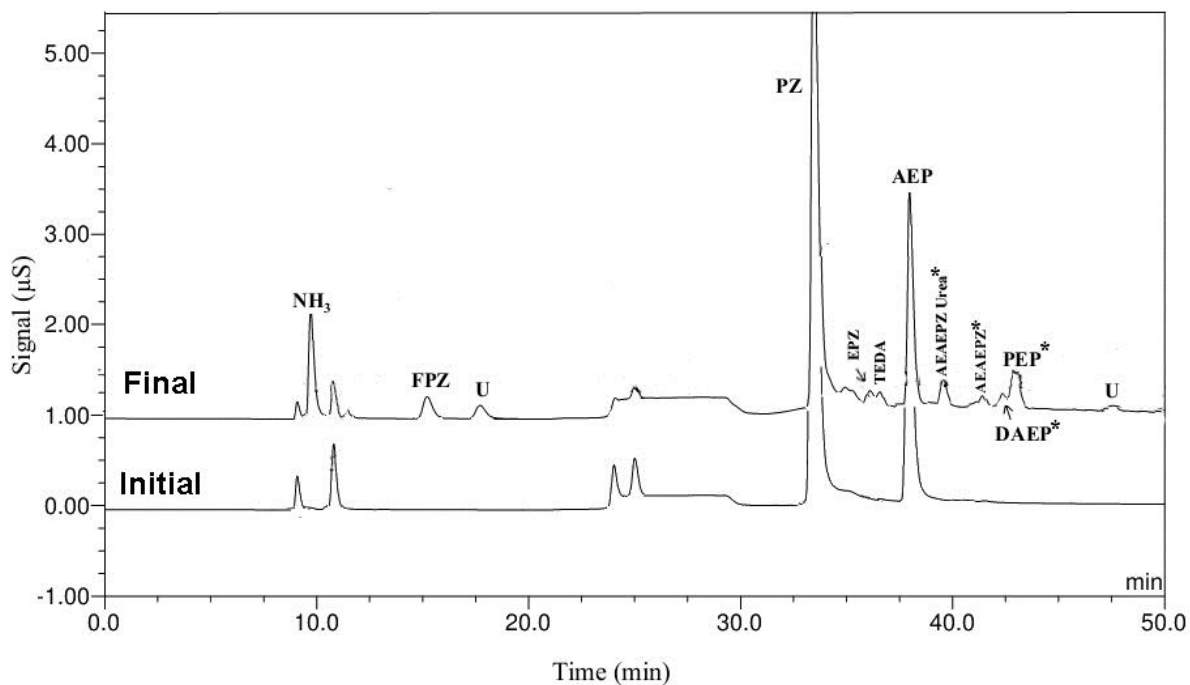


Figure 3.5: Cation IC chromatogram of the initial and final sample of 5 m PZ/2 m AEP at 175 °C (U: unknown).

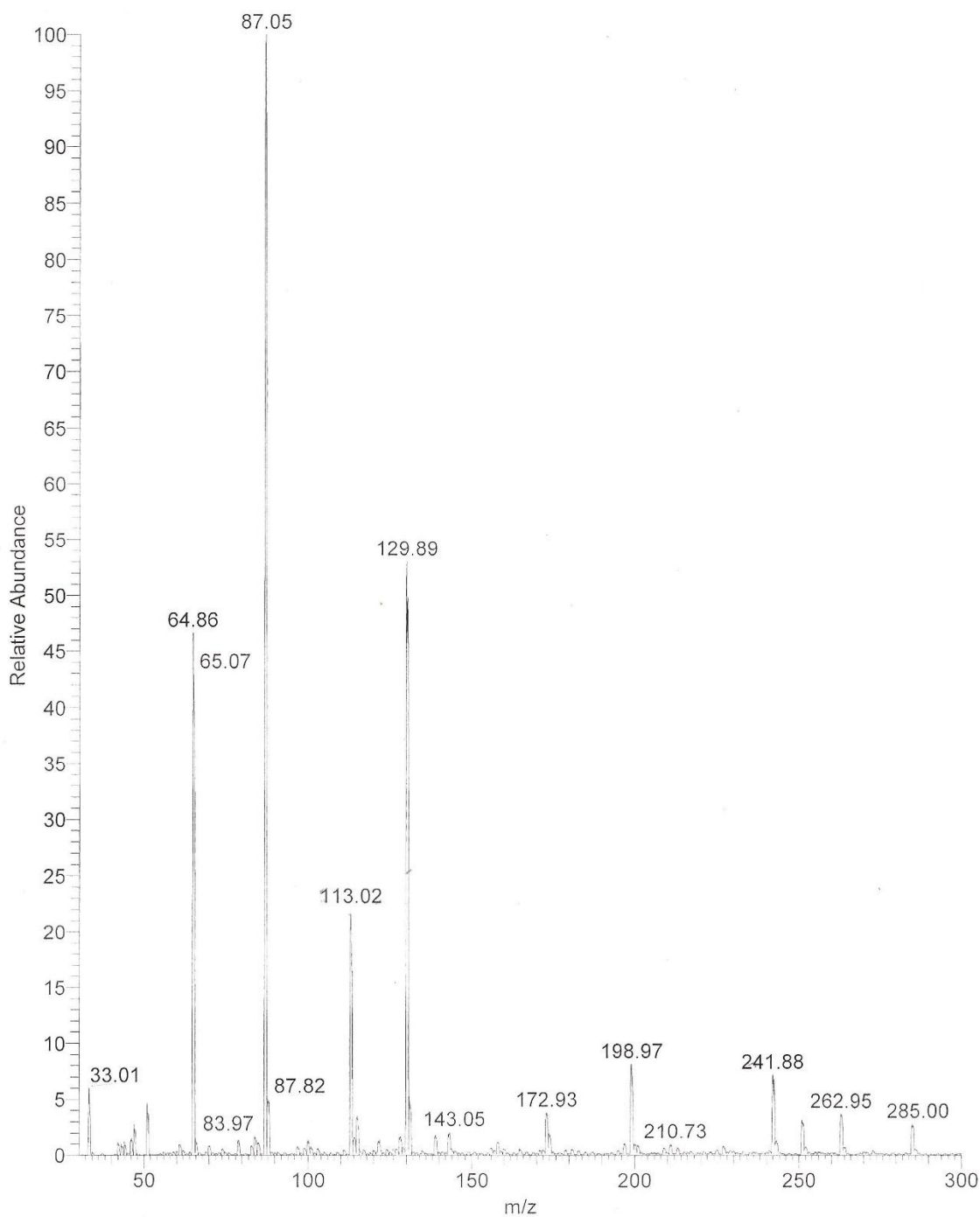


Figure 3.6: Mass spectrum for PZ/AEP degradation at 150°C for 5 weeks.

Carboxylate ions, known as heat stable salts, are also commonly produced in thermal degradation experiments and are quantified using anion IC. The carboxylate

ions produced in 5 m PZ/2 m AEP degradation are shown in Figure 3.7. The peak area of the two most abundant carboxylate ions (acetate and formate) identified by anion IC are shown in this figure along with their peak area after NaOH treatment. This value, labeled “Total anion”, represents the sum of all ion peaks identified by anion IC. “With NaOH” means the treatment of samples with an equal amount of 5 N NaOH for 24 hours, before further dilution and analysis. The difference between the original value and NaOH treatment value would represent the amount of amides of that carboxylate ion. As shown in Figure 3.7, formate was the dominant carboxylate ion produced in the degradation of PZ/AEP at 175 °C and the treatment of NaOH only led to about 10 % increase of carboxylate ions.

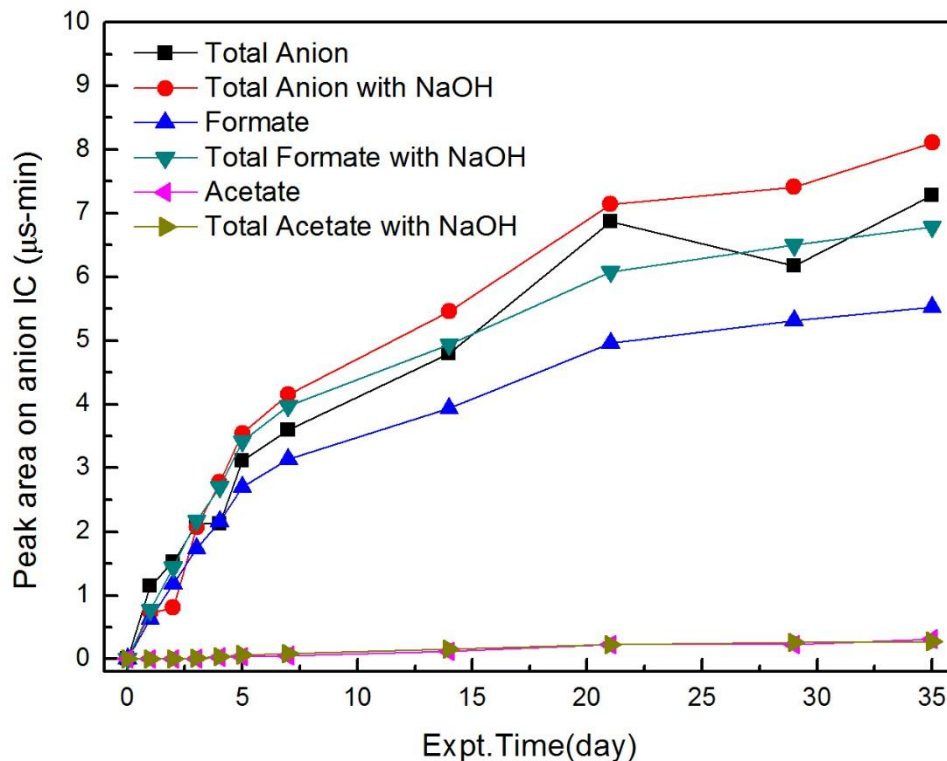


Figure 3.7: Production of carboxylate ions during thermal degradation of 5 m PZ/2 m AEP at 175°C

The thermal degradation products of 5 m PZ/2 m AEP at 175 °C are shown in Figure 3.8. As the retention time of TEDA is too close to that of 1-Ethyl PZ on cation ion chromatography, we quantified them as a combination. It can be seen that NH_4^+ and total formate, the sum of formate and N-Formyl PZ, were the two major products for the thermal degradation, while PEP, 1-Ethyl PZ, TEDA, total AEAEPZ, the sum of AEAEPZ and AEAEPZ Urea, and DAEP were the minor ones. The production of PEP and total AEAEPZ show a fast increase in the first week, followed by a quasi-steady state or very slow increase process in the rest 4 weeks, indicating PEP and AEAEPZ reach quasi-

equilibrium with PZ and AEP in the first week through reversible mechanisms. DAEP and 1-Ethyl PZ / TEDA started to show up after 2 weeks, indicating they are secondary thermal degradation products.

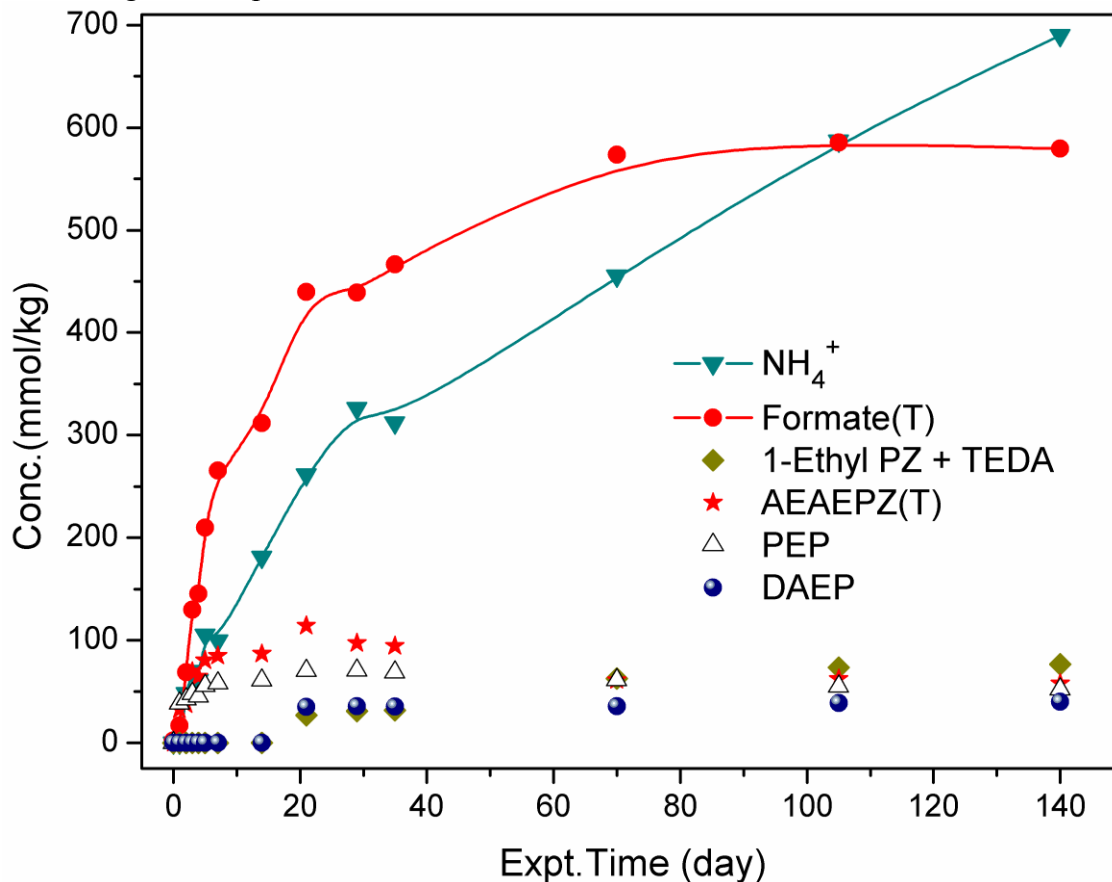


Figure 3.8: Degradation products from thermal degradation of 5 m PZ/2 m AEP with 0.3 mol CO₂/mol alkalinity at 175 °C.

PZ, AEP, and CO₂ loss are compared to the production of NH₄⁺ and total formate during thermal degradation of 5 m PZ/2 m AEP with 0.3 mol CO₂/mol alkalinity at 175 °C (Figure 3.9). The rate of PZ/AEP decrease is much larger than the rate of NH₄⁺ increase in the first week, indicating some degradation pathways that do not produce NH₄⁺ may also occur in the first week. This non-NH₄⁺ production pathway could be the

reaction between two PZ molecules to produce AEAEPZ and AEAEPZ urea (Freeman and Rochelle, 2011).

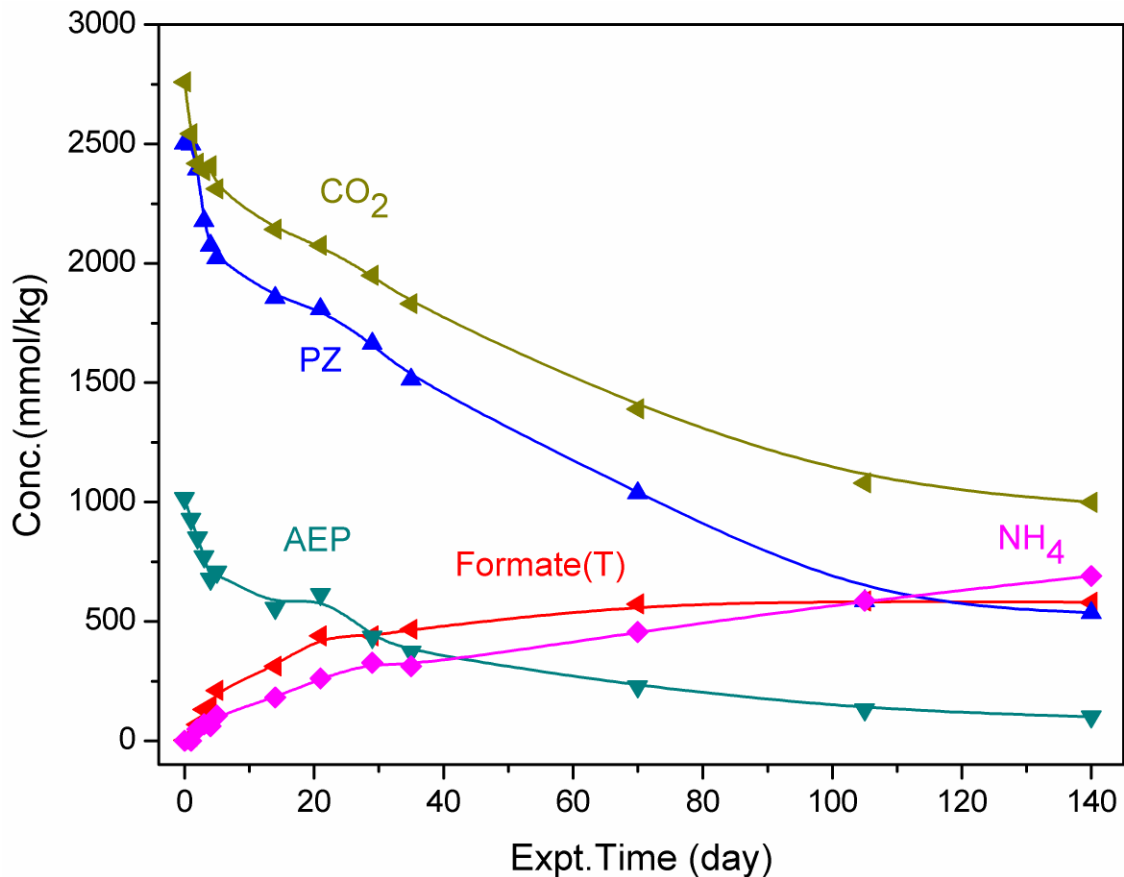


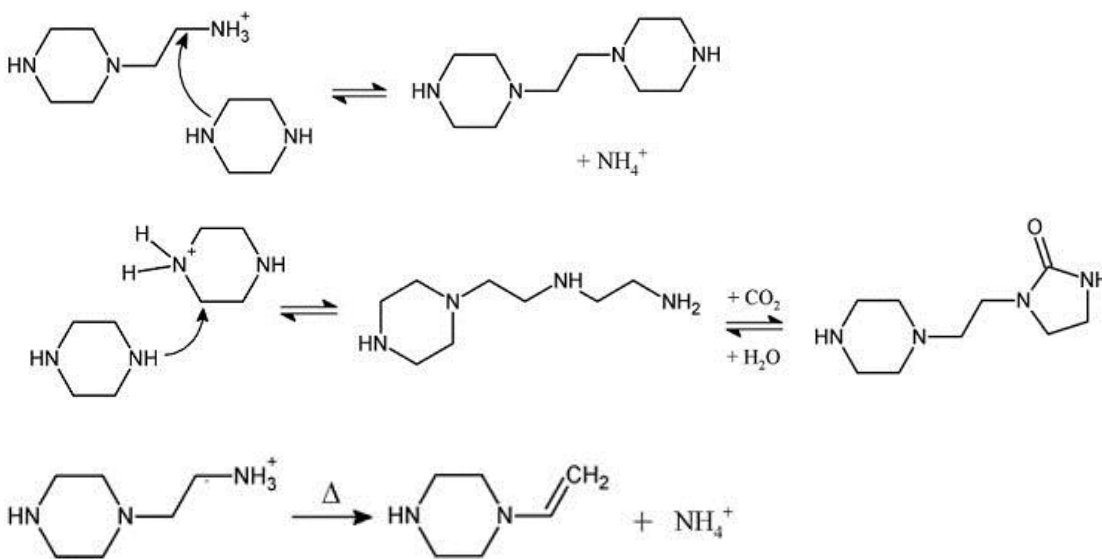
Figure 3.9: PZ, AEP, and CO₂ loss and generation of major degradation products for 5 m PZ/2 m AEP with 0.3 mol CO₂/mol alkalinity at 175 °C.

3.3.4 Proposed thermal degradation pathways of PZ/AEP

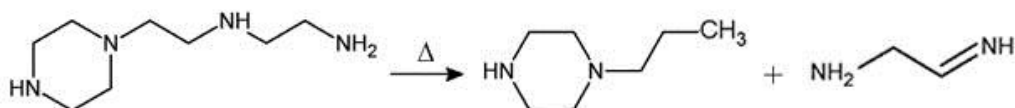
Thermal degradation of PZ/AEP produces a wide variety of molecules as degradation products as discussed above. The chemical mechanisms involved in producing each known product are not yet clear, but an overall set of pathways was developed that involves typical reactions and can describe the generation of the major products. This proposed set of pathways is meant for illustrative purposes and is not known at this time to be correct with complete confidence. The purpose is to suggest

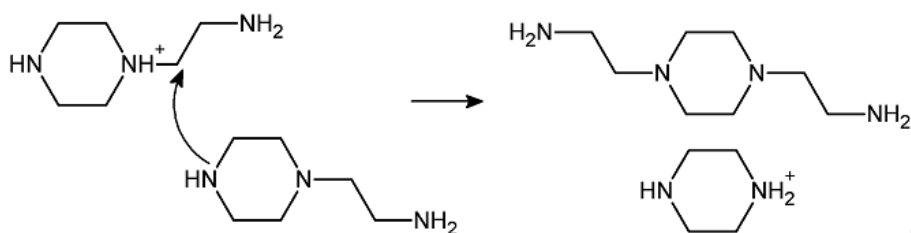
the types of reactions believed to be occurring. Further research into specific reaction pathways may disprove any portion of the mechanism.

Similar to pure PZ, the thermal degradation of PZ/AEP can be described as proceeding with four types of reactions: secondary SN₂ type substitution reactions, elimination reactions, urea generation, and formate generation from CO₂-containing molecules. At the early stage of degradation of PZ/AEP at 175 °C (within first week), the following three reactions may contribute significantly to the degradation.



In the late stage degradation of PZ/AEP, the following two reactions may contribute.





The formate and formyl amide (such as NPZ), which are also important degradation products, should result from CO_2 or CO_2 -containing molecules. Formate and formyl amide establish equilibrium once they are present in solution but it was not clear yet which was produced first and how it is generated from CO_2 or CO_2 -containing molecules.

3.4 OXIDATIVE DEGRADATION

Sexton (2009) and Freeman (2011) have shown that PZ oxidizes significantly slower than MEA under similar conditions, and that the generation rate of total formate (formate and formyl amides) can represent the oxidation rate of PZ under different conditions in low gas flow experiments. In this work, oxidation of 8 m PZ, 2 m AEP and 5 m PZ/2 m AEP at 70 °C in the presence of 0.1 mM Mn^{2+} and with the typical SSM mixture (0.4 mM Fe^{2+} , 0.05 mM Cr^{3+} and 0.1 mM Ni^{2+}), was investigated. The generation of total formate is shown in Figure 3.10, compared to that in 8 m PZ (Sexton and Rochelle 2009) and 7 m MEA in the absence of Mn^{2+} under similar conditions. It can be seen from Figure 3.10 that Mn^{2+} did not have a significant catalytic effect on the oxidation of PZ. In terms of the production of total formate, the oxidation of 2 m AEP and 5 m PZ/2 m AEP was comparable to that of 8 m PZ, but significantly slower than that of 7 m MEA.

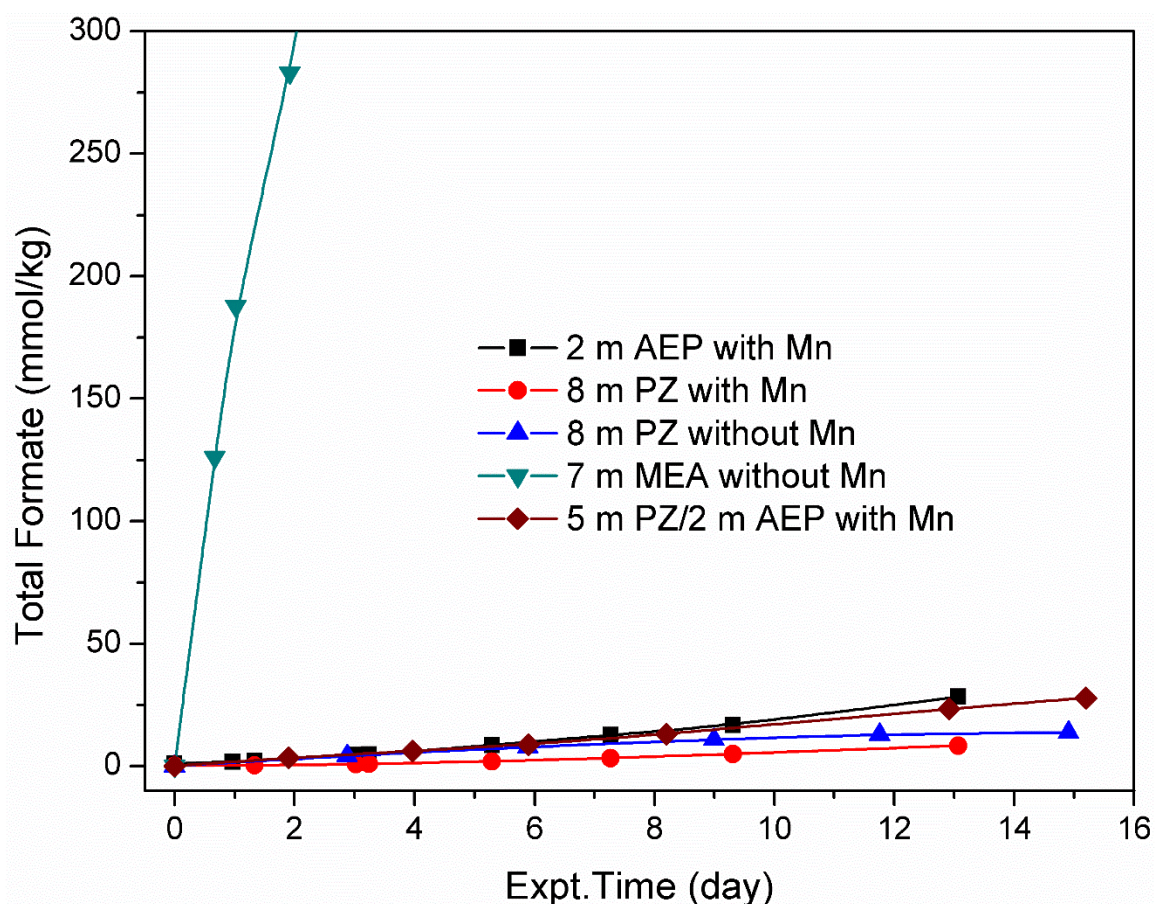


Figure 3.10: Comparison of total formate production in 5 m PZ/2 m AEP, 8 m PZ with Mn^{2+} , 8 m PZ without Mn^{2+} (Sexton and Rochelle, 2009), 2 m AEP and 7 m MEA (Sexton and Rochelle, 2009) at 70 °C.

3.5 NITROSAMINES

Nitrosamines, which are likely to be carcinogenic and can be formed through nitrosation of secondary amines (Fine et al., 2013), may be important when using amines containing secondary amine nitrogens in CO_2 capture. The formation of nitrosamines in 5 m PZ/2 m AEP was compared to that in 8 m PZ and 2 m AEP at 0.3 mol CO_2 /mol alkalinity and 100 °C (Figure 3.11). The normalized nitrosamine concentration is defined as the ratio of the nitrosamine concentration to the initial nitrite concentration. As can be seen from Figure 3.11, the formation rate of total nitrosamine (mono-nitroso-

PZ (MNPZ) and mono-nitroso-AEP (MNAEP)) in 5 m PZ/2 m AEP is similar to the formation rate of MNPZ in 8 m PZ. However, the formation of MNAEP in this blend is slower than that in 2 m AEP. This can be ascribed to the competition between PZ and AEP for CO₂ in blend. Compared to 2 m AEP, this blend produced less AEP carbamate species, which are likely to be the initiating species required for the initial reactions of nitrosation and first order to the formation rate of MNAEP (Fine et al., 2013).

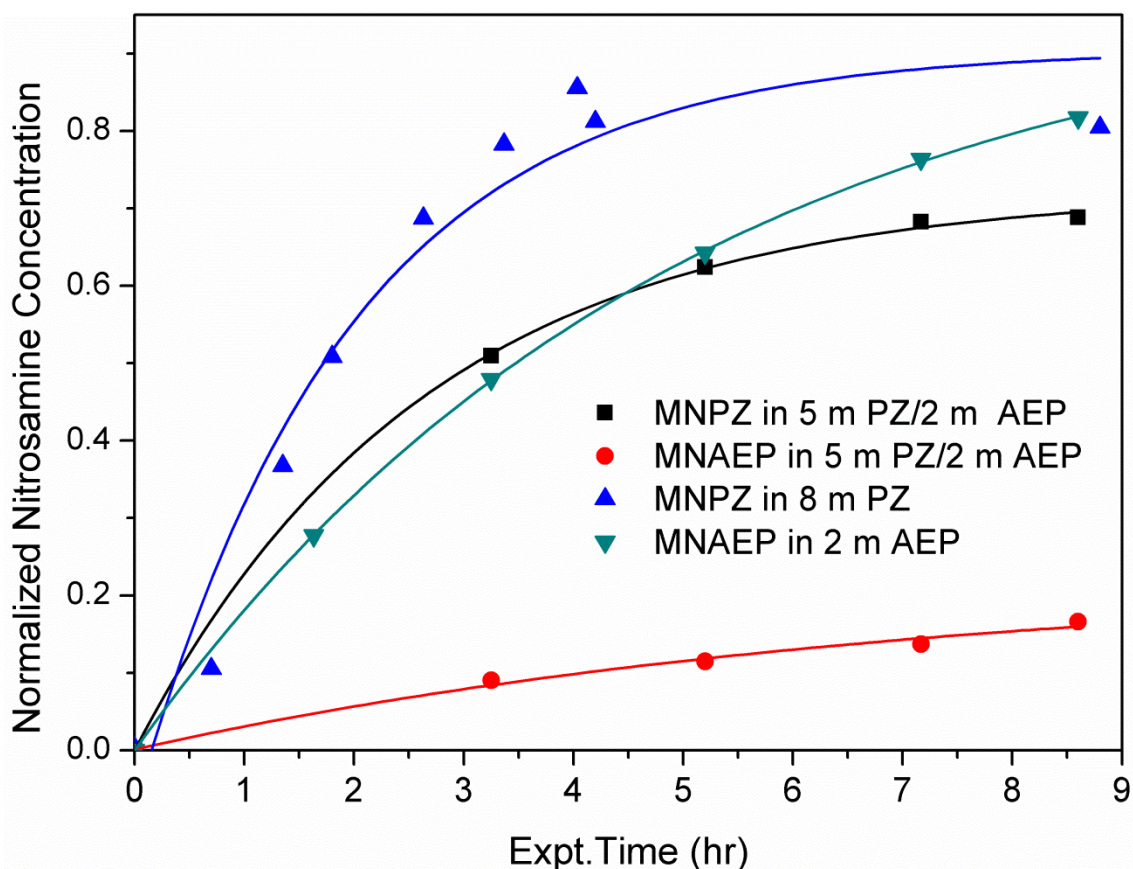


Figure 3.11: Nitrosamine formation in 5 m PZ/2 m AEP at 100 °C, compared to that in 8 m PZ (Fine et al., 2013) and 2 m AEP (the initial nitrite concentration was 40 mmol/kg solvent for all the three solvents).

The decomposition of nitrosamines in 5 m PZ/2 m AEP was investigated at 0.3 mol CO₂/mol alkalinity and 150 °C, compared to that in 8 m PZ and 2 m AEP under

similar conditions (Figure 3.12). As can be seen from Figure 3.9, the decomposition of MNPZ and MNAEP in 5 m PZ/2 m AEP is on the same scale as that of that of MNPZ in 8 m PZ. However, the decomposition of MNAEP in 5 m PZ/2 m AEP is much faster than that of MNAEP in 2 m AEP. This may be ascribed to the high amine concentration in this blend compared to 2 m AEP, though the mechanism for thermal decomposition of nitrosamine is still unclear at this moment. Together with the formation results, these results indicate that PZ/AEP may have a similar nitrosamine issue to individual PZ.

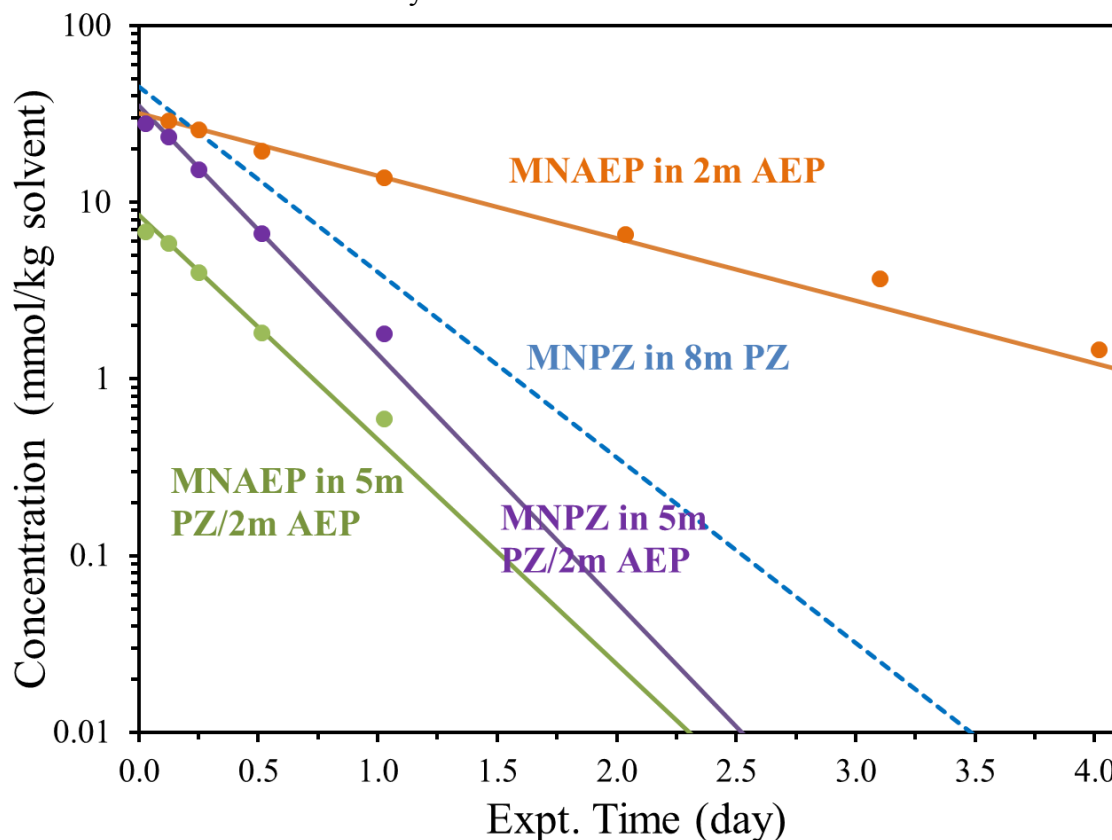


Figure 3.12: Nitrosamine decomposition in 5 m PZ/2 m AEP at 150 °C, compared to that in 8 m PZ (Fine et al., 2013) and 2 m AEP.

3.6 CO₂ SOLUBILITY

The CO₂ solubility in loaded 5 m PZ/2 m AEP was measured from 40 to 160 °C (Figure 3.13). CO₂ equilibrium partial pressure, P_{CO2} (Pa), was regressed using the

following empirical model as a function of temperature, T (K), and CO_2 loading, α (mol CO_2 /mol alkalinity), in the liquid phase.

$$\ln P_{\text{CO}_2} = 39.83 - 11105 \cdot \frac{1}{T} - 15.47 \cdot \alpha + 22167 \cdot \frac{\alpha^2}{T}$$

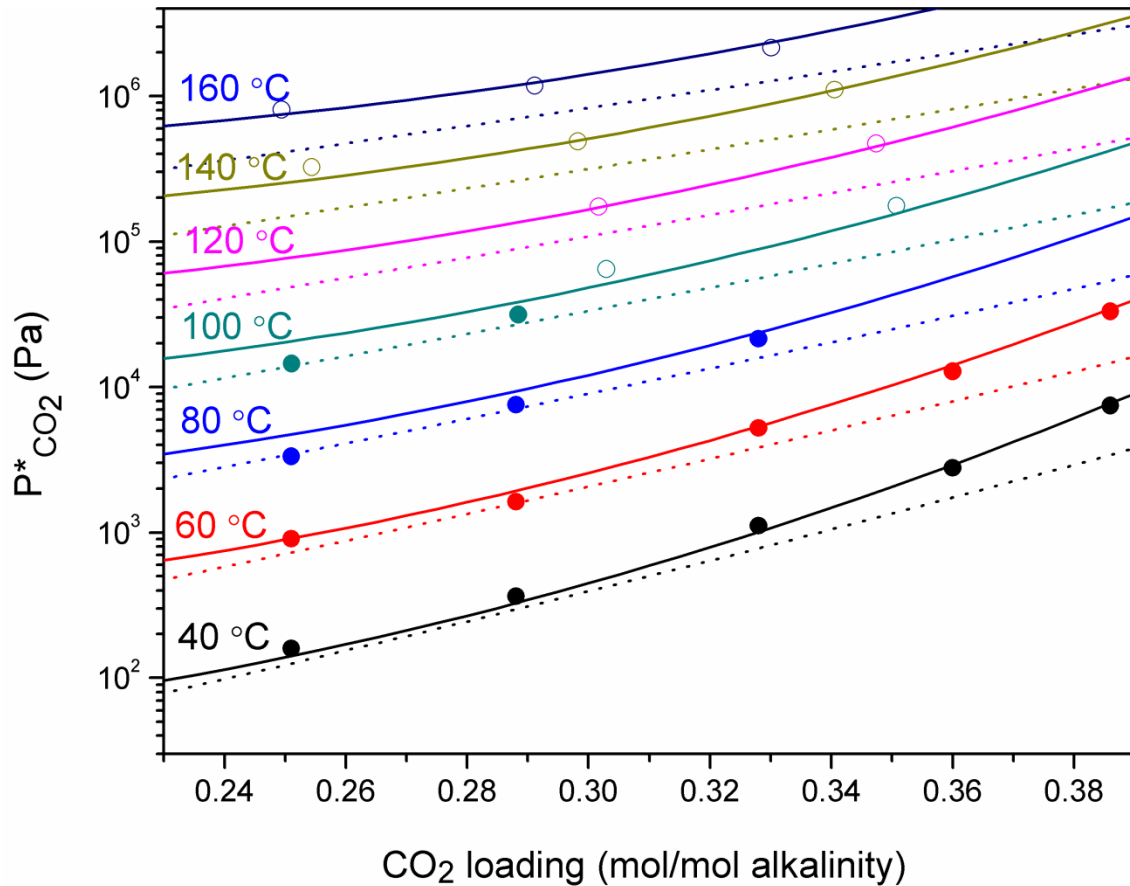


Figure 3.13: CO_2 solubility for 5 m PZ/2 m AEP (Solid lines: 5 m PZ/2 m AEP equation model; Solid circles: measured data for 5 m PZ/2 m AEP using WWC; Open circles: measured data for 5 m PZ/2 m AEP using SA; Dashed lines: 8 m PZ equation model from Xu (2011)).

The CO_2 partial pressure of 8 m PZ is also given in Figure 3.13 for comparison. From Figure 3.13 we can see that CO_2 partial pressure of 5 m PZ/2 m AEP is consistently higher than that of 8 m PZ from 40 to 160 °C, indicating a lower CO_2 solubility in this blend. Based on the difference in the equilibrium CO_2 partial pressure from 5 to 0.5 kPa at 40 °C, the working capacity of 5 m PZ/2 m AEP (0.68 mole per kg amines + water) is

lower than that of 8 m PZ (Li et al., 2013) (0.86 mole per kg amines + water), but still much higher than that of 7 m MEA (0.50 mole per kg amines + water) (Li et al., 2013).

3.7 ABSORPTION RATE

CO₂ absorption rate into 5 m PZ/2 m AEP was studied in a wetted wall column from 20 to 100 °C with loading from 0.25 to 0.39 mol CO₂/mol alkalinity. The liquid-film mass coefficients (kg') of CO₂ absorption into 5 m PZ/2 m AEP are shown in Figure 3.14. To compare kg' in 5 m PZ/2 m AEP to that in 8 m PZ on the same basis, the rate data are plotted against partial pressure of CO₂ instead of CO₂ loading. To compare kg' at variable temperature, the rate data of 5 m PZ/2 m AEP at 20 to 100 °C are plotted as a function of the equilibrium partial pressure of CO₂ at 40 °C. At 40 °C the rate in the blend is similar to that in 8 m PZ. Similar to other amines studied for CO₂ capture (Li et al., 2013), temperature has a negative effect on CO₂ absorption rate into 5 m PZ/2 m AEP, especially at rich CO₂ loading.

CO₂ cyclic capacity, CO₂ absorption rate, the heat of CO₂ absorption predicted from CO₂ solubility measurement, and the maximum stripper operating temperature T_{max} of 5 m PZ/2 m AEP are summarized in Table 3.3 and compared to other conventional solvents (Li et al., 2013).

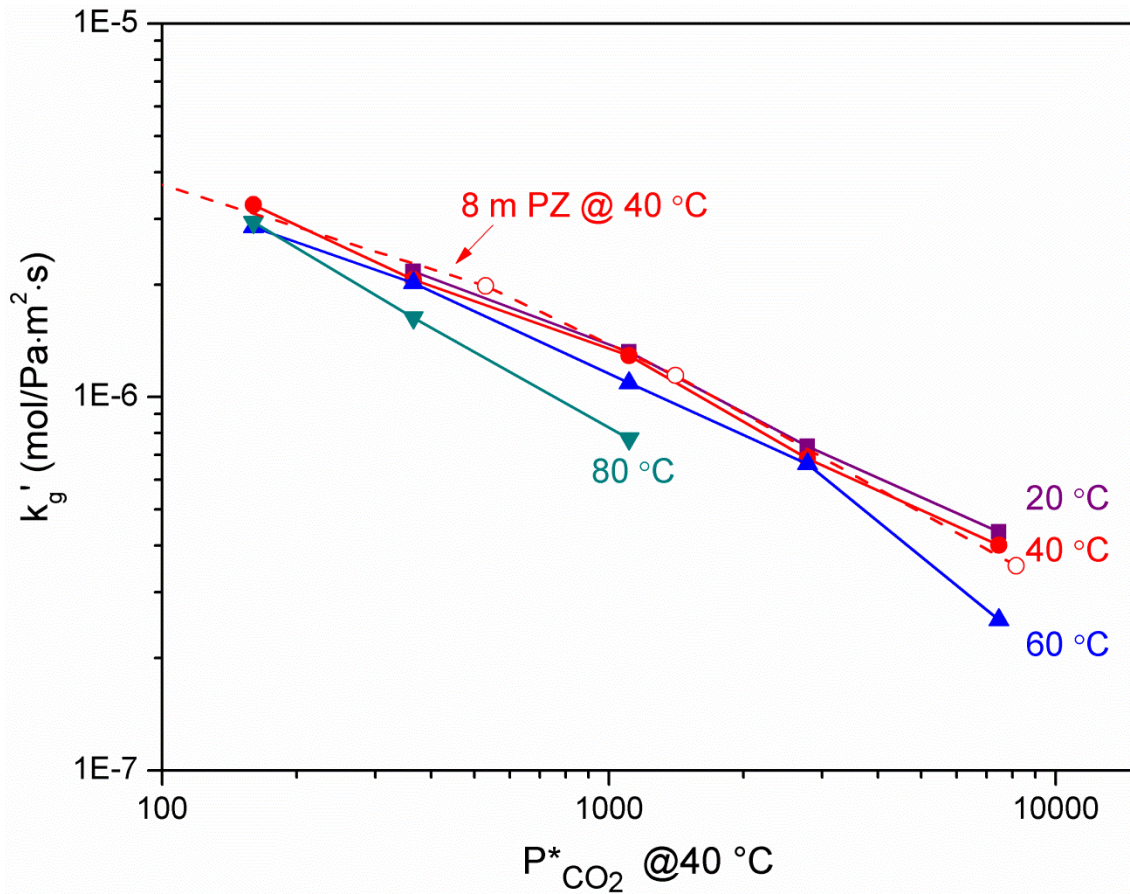


Figure 3.14: Mass transfer coefficients (k_g') in 5 m PZ/2 m AEP (solid lines) from 20 to 80 °C, compared to that in 8 m PZ (dashed line) at 40 °C.

Table 3.3: Summary of capacity, absorption rate, heat of absorption, and maximum stripper temperature for 5 m PZ/ 2 m AEP and other conventional amines (Li et al., 2013).

Amine	Capacity mol/kg	$k_g'_{avg}$ (40 °C) mol/Pa s m ²	- $H_{abs-avg}$ (40 °C) kJ/mol	T_{max} °C
5 m PZ / 2 m AEP	0.68	8.1	71	155
5 m PZ / 2.3 m AMP	0.70	7.5	71	128
5 m PZ / 5 m MDEA	0.98	8.5	69	138
8 m PZ	0.86	8.5	67	163
7 m MEA	0.50	4.3	72	121

Chapter 4: Thermodynamic modeling of PZ/AEP

4.1 THERMODYNAMIC FRAMEWORK

The thermodynamic model built for PZ-AEP-H₂O-CO₂ in this work is based on the model for PZ-H₂O-CO₂ (“Independence” model) developed by Frailie (2011) in Aspen Plus[®]. Therefore, the basic thermodynamic framework is identical to the “Independence” model: using eNRTL model for liquid phase behavior and Soave–Redlich–Kwong (SRK) equation for gas phase behavior.

4.1.1 Aqueous-phase chemical equilibrium

AEP is a tri-amine with primary, secondary, and tertiary amine groups in its structure, leading to various protonated and carbamate species. The third pK_a of AEP was reported to be below 4 at 25–50 °C (Pagano et al., 1961), while the normal pH value in CO₂-loaded amine solution at the rich loading is typically well above 8. Therefore, the amount of tri-protonated AEP is extremely small in loaded solutions and it is excluded from consideration in this work. Both the primary and secondary amino groups of AEP can connect with a carboxyl group, leading to two isomers of AEP carbamate. Table 4.1 lists potential species in PZ-AEP-H₂O-CO₂. For simplicity, protonated species are not listed. To differentiate the carbon nuclei with different electronic environment, they are numbered for different species present.

Table 4.1: Molecular structure of the compounds in CO₂-loaded PZ-AEP aqueous solutions.

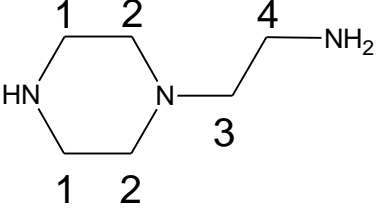
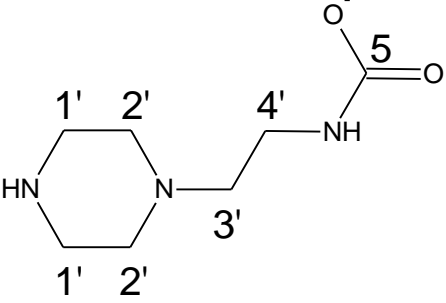
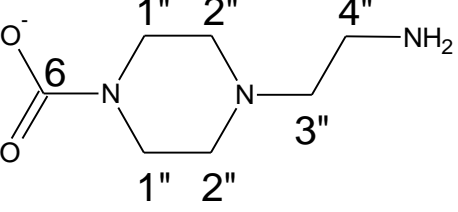
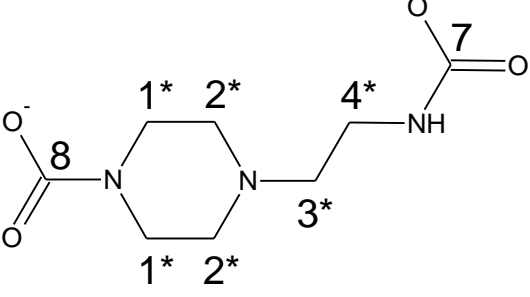
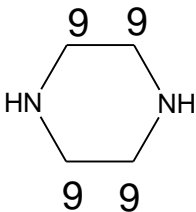
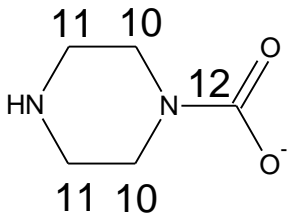
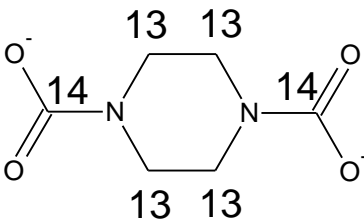
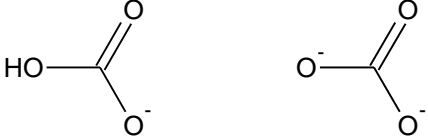
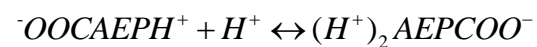
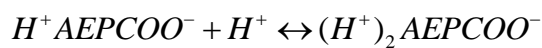
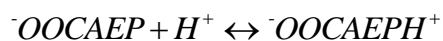
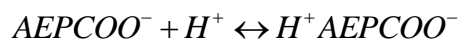
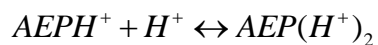
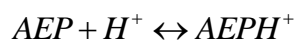
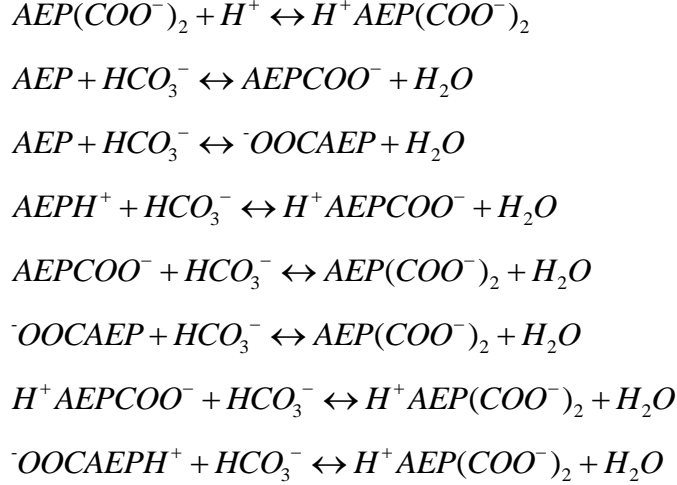
Name	Molecular Structure
AEP	
AEP ⁻ COO ⁻	
⁻ OOCAEP	
AEP(COO ⁻) ₂	

Table 4.1: continued

PZ	
PZCOO ⁻	
PZ(COO ⁻) ₂	
HCO ₃ ⁻ / CO ₃ ²⁻	

Besides the aqueous-phase chemical equilibrium reactions set up in the “Independence” model for PZ-H₂O-CO₂, the following reactions involving AEP species were used in this study.





AEP is an existing component in the Aspen Plus® databank. Other AEP-related species were added as new components. Following the treatment in the “Independence” model, AEP and zwitterions ($H^+AEPCOO^-$ and $^-OOCAEPH^+$) were modeled as Henry’s components. Zwitterions were assigned with an extremely low Henry’s constant as they are expected to be non-volatile.

4.1.2 Reference state and units

In the “Independence” model, two different reference states are used depending on whether the species is a solvent or solute and we follow the same treatment in this work. The symmetric convention is applied for water as a solvent with the reference state as pure solvent at the system temperature and pressure:

$$\gamma_s \rightarrow 1 \text{ as } x_s \rightarrow 1 \quad (1)$$

The asymmetric convention was used for solutes (AEP, zwitterion, and ions) with the reference state as infinite dilution in water at the temperature and pressure of the system:

$$\gamma_i^* \rightarrow 1 \text{ as } x_i \rightarrow 0 \quad (2)$$

where γ_s is the symmetric activity coefficient of solvent and γ_i^* the asymmetric activity coefficient of solutes.

4.1.3 Reaction equilibrium

The reaction equilibrium constant is expressed as follows.

$$K_j = \prod_i a_i^{v_{ij}} = \prod_i (x_i \gamma_i)^{v_{ij}} \quad (3)$$

where K_j is the equilibrium constant of reaction j on a mole fraction scale; a_i is the activity of component i ; v_{ij} is the stoichiometric coefficient of component i in reaction j ; x_i and γ_i are the mole fraction and the activity coefficient of component i , respectively.

The chemical equilibrium constant was determined from the Gibbs free energy change of the reaction.

$$-\ln K_j = \frac{\Delta G_j(T)}{RT} \quad (4)$$

where $\Delta G_j(T)$ is the Gibbs free energy change for reaction j at system temperature; $\Delta G_j(T)$ is defined as the difference between the Gibbs free energy of formation of the products and reactants at their reference state, $G_i(T)$, weighted by their stoichiometric coefficients.

$$\Delta G_j(T) = \sum_i v_{ij} G_i(T) \quad (5)$$

For solvents (water in this work), the Gibbs free energy of formation in their reference state (pure solvent) was calculated from that of ideal gas and the departure function:

$$G_s(T) = G_s^{ig}(T) + \Delta G_s^{ig \rightarrow l}(T) \quad (6)$$

The ideal gas Gibbs free energy of formation of solvent, $G_s^{ig}(T)$, was calculated from the following equation:

$$G_s^{ig}(T) = \Delta_f H_{s,298.15}^{ig} + \int_{298.15}^T C_{P,s}^{ig} dT - T \times \left(\frac{\Delta_f H_{s,298.15}^{ig} - \Delta_f G_{s,298.15}^{ig}}{298.15} + \int_{298.15}^T \frac{C_{P,s}^{ig}}{T} dT \right) \quad (7)$$

where $\Delta_f H_{s,298.15}^{ig}$ and $\Delta_f G_{s,298.15}^{ig}$ are ideal gas enthalpy of formation and ideal gas Gibbs free energy of formation of solvent s at 298.15 K, respectively, and $C_{P,s}^{ig}$ the ideal gas heat capacity of solvent s. The standard state thermodynamic properties of water ($\Delta_f H_{s,298.15}^{ig}$, $C_{P,s}^{ig}$, and $\Delta_f G_{s,298.15}^{ig}$) exist in the Aspen Plus® databank. The Gibbs free energy departure function for water was obtained from the ASME steam table.

For molecular solutes (CO_2 , AEP, and $\text{H}^+\text{AEP}\text{COO}^-$), the Gibbs free energy in their reference state (infinite dilution in aqueous phase), $G_i^{\infty,aq}(T)$, was calculated from Henry's law:

$$G_i^{\infty,aq}(T) = G_i^{ig}(T) + RT \ln \left(\frac{H_{i,s}(T,P)}{P^{ref}} \right) \quad (8)$$

where $H_{i,s}(T,P)$ is the Henry's constant of molecular solute i in solvent s at system temperature T and pressure P; P^{ref} the reference pressure of 1 bar, and $G_i^{ig}(T)$ the ideal gas Gibbs free energy of formation of molecular solute i, which is calculated in the same way as that for solvent:

$$G_i^{ig}(T) = \Delta_f H_{i,298.15}^{ig} + \int_{298.15}^T C_{P,i}^{ig} dT - T \times \left(\frac{\Delta_f H_{i,298.15}^{ig} - \Delta_f G_{i,298.15}^{ig}}{298.15} + \int_{298.15}^T \frac{C_{P,i}^{ig}}{T} dT \right) \quad (9)$$

where $\Delta_f H_{i,298.15}^{ig}$ and $\Delta_f G_{i,298.15}^{ig}$ are ideal gas enthalpy of formation and ideal gas Gibbs free energy of formation of molecular solute i at 298.15 K, respectively, and $C_{P,i}^{ig}$ is the ideal gas heat capacity of molecular solute i.

$\Delta_f H_{i,298.15}^{ig}$, $\Delta_f G_{i,298.15}^{ig}$, and $C_{P,i}^{ig}$ of CO_2 and AEP exist in the Aspen Plus® databank. The difference of $\Delta_f H_{i,298.15}^{ig}$ and $\Delta_f G_{i,298.15}^{ig}$ between $\text{H}^+\text{AEP}\text{COO}^-/\text{OOCAEPH}^+$ and the parent amine, AEP, were assumed to be the same as the difference between $\text{H}^+\text{PZ}\text{COO}^-$ and PZ in the Independence model. These estimated values were

used as the initial guess in the regression of the data of CO₂ solubility in aqueous AEP solution, from which the final values of these parameters of H⁺AEP⁻COO⁻ and ⁻OOCAEPH⁺ were obtained. $C_{P,i}^{ig}$ of H⁺AEP⁻COO⁻ and ⁻OOCAEPH⁺ were estimated based on the ratio of their molecular weight to AEP. $C_{P,i}^{ig}$ of AEP, H⁺AEP⁻COO⁻, and ⁻OOCAEPH⁺ were fixed in future regressions.

The Henry's constant, $H_{i,s}(T, P)$, was calculated from

$$H_{i,s}(T, P) = H_{i,s}(T, P_s^{*,l}) \exp\left(\frac{1}{RT} \int_{P_s^{*,l}}^P V_{i,s}^{\infty} dP\right) \quad (10)$$

where $H_{i,s}(T, P_s^{*,l})$ is the Henry's constant of molecular solute *i* in solvent *s* at system temperature *T* and the solvent vapor pressure; $P_s^{*,l}$ (obtained from the Antoine model), and $V_{i,s}^{\infty}$ the partial molar volume of molecular solute *i* at infinite dilution in solvent *s* at *T* and *P* (calculated from the Brelvi-O'Connell model by using their critical properties). The Poynting pressure correction factor (the exponent term) accounts for the effect of pressure on Henry's constant, and is almost unity and can be ignored at low pressures. $H_{i,s}(T, P_s^{*,l})$ was calculated using the following correlation in Aspen Plus[®]:

$$\ln H_{i,s} = a_{i,s} + \frac{b_{i,s}}{T} + c_{i,s} \times \ln(T) + d_{i,s} \times T \quad (11)$$

The Henry's coefficients, $a_{i,s}$, $b_{i,s}$, $c_{i,s}$, $d_{i,s}$ of CO₂ in water are available in the Aspen Plus[®] databank, while the Henry's coefficients of AEP in water were obtained from regression of aqueous AEP volatility data.

For ionic solutes, the Gibbs free energy of formation in their reference state (infinite dilution in aqueous phase), $G_i^{\infty, aq}(T)$, at system temperature were calculated from the enthalpy of formation and Gibbs free energy of formation in aqueous-phase infinite dilution at 298.15 K, and the heat capacity in aqueous-phase infinite dilution.

$$G_i^{\infty,aq}(T) = \Delta_f H_{i,298.15}^{\infty,aq} + \int_{298.15}^T C_{P,i}^{\infty,aq} dT - T \times \left(\frac{\Delta_f H_{i,298.15}^{\infty,aq} - \Delta_f G_{i,298.15}^{\infty,aq}}{298.15} + \int_{298.15}^T \frac{C_{P,i}^{\infty,aq}}{T} dT \right) + RT \ln \left(\frac{1000}{M_w} \right) \quad (12)$$

The term $RT \ln(1000/M_w)$ is added because $\Delta_f G_{i,298.15}^{\infty,aq}$, as reported in the literature, is based on molality scale, while $G_i^{\infty,aq}(T)$ is based on mole fraction scale. The standard state thermodynamic properties, $\Delta_f H_{i,298.15}^{\infty,aq}$, $\Delta_f G_{i,298.15}^{\infty,aq}$, and $C_{P,i}^{\infty,aq}$, for AEP-related ionic species are not available in the Aspen Plus® databank. The $\Delta_f H_{i,298.15}^{\infty,aq}$ and $\Delta_f G_{i,298.15}^{\infty,aq}$ of AEPH^+ and $\text{AEP}(\text{H}^+)_2$ were calculated from the protonation reactions of AEPH^+ and $\text{AEP}(\text{H}^+)_2$ measured by Pagano (1961).

$$\Delta_f G_{\text{AEPH}^+, 298.15}^{\infty,aq} = \Delta_f G_{\text{AEP}, 298.15}^{\infty,aq} + \Delta_r G_i = \Delta_f G_{\text{AEP}, 298.15}^{\infty,aq} - RT \ln K_{m,i} \quad (13)$$

$$\Delta_f H_{\text{AEPH}^+, 298.15}^{\infty,aq} = \Delta_f H_{\text{AEP}, 298.15}^{\infty,aq} + \Delta_r H_i \quad (14)$$

$$\Delta_f G_{\text{AEP}(\text{H}^+)_2, 298.15}^{\infty,aq} = \Delta_f G_{\text{AEPH}^+, 298.15}^{\infty,aq} + \Delta_r G_i = \Delta_f G_{\text{AEP}, 298.15}^{\infty,aq} - RT \ln K_{m,i} \quad (15)$$

$$\Delta_f H_{\text{AEP}(\text{H}^+)_2, 298.15}^{\infty,aq} = \Delta_f H_{\text{AEPH}^+, 298.15}^{\infty,aq} + \Delta_r H_i \quad (16)$$

where $\Delta_r G_i$, $\Delta_r H_i$, and $K_{m,i}$ are Gibbs free energy change, enthalpy change, and molality scale protonation constants of a certain reaction; $\Delta_f G_{\text{AEP}, 298.15}^{\infty,aq}$ and $\Delta_f H_{\text{AEP}, 298.15}^{\infty,aq}$ are Gibbs free energy of formation and enthalpy of formation of AEP in aqueous-phase infinite dilution at 298.15 K, which can be obtained from Henry's law as follows:

$$\Delta_f G_{\text{AEP}, 298.15}^{\infty,aq} = \Delta_f G_{\text{AEP}, 298.15}^{ig} + R * 298.15 * \left(\frac{H_{\text{AEP}, \text{H}_2\text{O}}}{P^{ref}} \right) - RT \ln \left(\frac{1000}{M_w} \right) \quad (17)$$

$$\Delta_f H_{\text{AEP}, 298.15}^{\infty,aq} = \Delta_f H_{\text{AEP}, 298.15}^{ig} + R \frac{\partial \ln H_{\text{AEP}, \text{H}_2\text{O}}}{\partial (1/T)} \quad (18)$$

The term $RT \ln(1000/M_w)$ is subtracted because $\Delta_f G_{i,298.15}^{\infty,aq}$ in Aspen Plus® is based on molality scale, while $\Delta_f G_{i,298.15}^{ig}$ (as provided in the databank) is based on mole fraction scale. The conversion of equilibrium constants from molality scale to mole fraction scale can be found in Hilliard (Hilliard 2008).

$\Delta_f H_{i,298.15}^{\infty, aq}$ and $\Delta_f H_{i,298.15}^{\infty, aq}$ of other AEP-related ions were initially estimated based on the assumption that the difference between AEP-related species is the same as the difference between corresponding PZ-related species. For example, we assume:

$$\Delta_f H_{AEP-CO_2}^{\infty, aq} - \Delta_f H_{AEP}^{\infty, aq} = \Delta_f H_{PZ-CO_2}^{\infty, aq} - \Delta_f H_{PZ}^{\infty, aq}$$

and

$$\Delta_f H_{AEP-CO_2}^{\infty, aq} - \Delta_f H_{AEP}^{\infty, aq} = \Delta_f H_{PZ-CO_2}^{\infty, aq} - \Delta_f H_{PZ}^{\infty, aq}$$

These values were used as an initial guess in the regression of the CO₂ solubility in aqueous AEP solution, from which the final value of these parameters was obtained. $C_{P,i}^{\infty, aq}$ of AEP was assumed to be the same as $C_{P,i}^{ig}$ of AEP, and then $C_{P,i}^{\infty, aq}$ of other AEP species was estimated based on the ratio of their molecular weight to AEP. $C_{P,i}^{\infty, aq}$ of all AEP species were fixed in future regressions.

4.1.4 Vapor-liquid phase equilibrium

Phase equilibrium governs the distribution of molecular species between the vapor and liquid phase. In the activity coefficient approach, the basic vapor-liquid equilibrium relationship for solvent is represented by:

$$\phi_s^V y_s P = \gamma_s x_s P_s^{*,l} \exp\left(\frac{1}{RT} \int_{P_s^{*,l}}^P V_s^{*,l} dP\right) \quad (19)$$

where ϕ_s^V is the vapor phase fugacity coefficient of solvent s, γ_s the symmetric activity coefficient of solvent s, $P_s^{*,l}$ the solvent vapor pressure at system temperature, and $V_s^{*,l}$ the liquid pure component molar volume of solvent s calculated from the Rackett model.

For molecular solutes, Henry's Law was used to determine vapor-liquid equilibrium:

$$\phi_i^V y_i P = \gamma_i^* x_i H_{i,s}(T, P_s^{*,l}) \exp\left(\frac{1}{RT} \int_{P_s^{*,l}}^P V_{i,s}^{\infty} dP\right) \quad (20)$$

where γ_i^* is the symmetric activity coefficient of component i.

4.1.5 Vapor phase behavior

Vapor phase behavior was modeled using the Redlich-Kwong-Soave (RKS) equation of state:

$$P = \frac{RT}{V-b} - \frac{a}{V(V-b)} \quad (21)$$

T and P represent the temperature and pressure of the vapor phase and R represents the gas constant. The attraction between molecules and their size are represented in the equation by parameters a and b respectively, which are calculated from critical properties.

4.1.6 System non-idealities

Vapor phase non-idealities (fugacity) are calculated using the SRK equation of state. Liquid phase non-idealities (activity) are calculated using the eNRTL model. The use of the eNRTL model in amine/acid gas systems has been described previously by Posey (1997) and Frailie (2011). The basic postulate of this model is that the excess Gibbs energy of an aqueous electrolyte system can be written as the sum of three contributions: the NRTL term (related to the local ion-molecule, ion-ion, and molecule-molecule interactions that exist in the immediate neighborhood of any species), the PDH term (related to the long-range ion-ion interactions that exist beyond the immediate neighborhood of a central ionic species) and the Born term (accounts for the excess Gibbs energy of transfer from infinite dilution in the mixed solvent to infinite dilution in the aqueous phase).

$$g_i^{ex*} = g_{PDH,i}^{ex*} + g_{Born,i}^{ex} + g_{NRTL,i}^{ex*} \quad (22)$$

Accordingly,

$$\ln \gamma_i = \ln \gamma_i^{PDH} + \ln \gamma_i^{Born} + \ln \gamma_i^{NRTL} \quad (23)$$

The adjustable parameters for the eNRTL model include the pure component dielectric constant coefficient, Born radius of ionic species, and NRTL parameters for molecule-molecule, molecule-electrolyte, and electrolyte-electrolyte pairs. The NRTL

parameters are the nonrandomness factors and binary interaction parameters. Following the treatment for PZ in the Independence model, dielectric constants of AEP are assumed to be the same as MEA; ionic radii were assigned default values of 3 Å; the nonrandomness factor was fixed at 0.3 for molecule-molecule pairs and 0.2 for molecule-electrolyte and electrolyte-electrolyte pairs, and binary interaction parameters for electrolyte-electrolyte pairs were set to zero. Therefore, the only adjustable parameters of the eNRTL model in this work were binary interaction parameters for molecule-molecule pairs and for electrolyte-molecule pairs, as expressed in the following relationships as a function of temperature.

Molecule-molecule binary interaction parameters:

$$\tau_{mm'} = A_{mm'} + \frac{B_{mm'}}{T} + C_{mm'} \ln(T) + D_{mm'} T \quad (24)$$

Electrolyte-molecule (or molecule-electrolyte) binary interaction parameters:

$$\tau_{x,y} = E_{x,y} + \frac{F_{x,y}}{T} \quad (25)$$

$$\tau_{x,y} = \tau_{ca,m} \text{ OR } \tau_{m,ca} \quad (26)$$

Subscripts and indices of m , c , and a refer to molecules, cations, and anions, respectively. $\tau_{mm'}$, $\tau_{ca,m}$, and $\tau_{m,ca}$ can be obtained from the regression of amine volatility data and CO₂ solubility data.

The parameters used in this model are summarized in Table 4.2. All model parameters not mentioned in Table 4.2 were either from the “Independence” model or set to Aspen Plus® default values.

Table 4.2: Summary of model parameters.

Parameters	Component	Source	Data for regression
$\Delta_f G_{s,29815}^{ig}$	AEP	Aspen Plus® Databank	—
	H ⁺ AEP ⁻ COO ⁻ / -OOCAEPH ⁺	Regression	VLE and NMR for AEP-H ₂ O-CO ₂
$\Delta_f H_{s,29815}^{ig}$	AEP	Aspen Plus® Databank	—
	H ⁺ AEP ⁻ COO ⁻ / -OOCAEPH ⁺	Regression	VLE and NMR for AEP-H ₂ O-CO ₂
$C_{P,s}^{ig}$	AEP	Aspen Plus® Databank	—
	H ⁺ AEP ⁻ COO ⁻ / -OOCAEPH ⁺	Ratio to $C_{P,s}^{ig}$ of AEP	—
$\Delta_f G_{i,29815}^{\infty,aq}$	AEPH ⁺ / AEP(H ⁺) ₂	(Pagano et al., 1961)	—
	Other AEP ions	Regression	VLE and NMR for AEP-H ₂ O-CO ₂
$\Delta_f H_{i,29815}^{\infty,aq}$	AEPH ⁺ / AEP(H ⁺) ₂	(Pagano et al., 1961)	—
	Other AEP ions	Regression	VLE and NMR for AEP-H ₂ O-CO ₂
$C_{P,i}^{\infty,aq}$	All AEP species	Ratio to $C_{P,s}^{ig}$ of AEP	—
Henry's constant	AEP/H ₂ O	Regression	Volatility of AEP
	H ⁺ AEP ⁻ COO ⁻ / H ₂ O -OOCAEPH ⁺ / H ₂ O	Assumed same as H ⁺ PZCOO ⁻ / H ₂ O	—
Dielectric constant	AEP	Assumed same as PZ	—
NRTL binary interaction parameters	AEP/H ₂ O	Regression	Volatility of AEP
	AEP cation, PZ anion / H ₂ O	Regression	VLE for PZ-AEP- H ₂ O-CO ₂
	PZ cation, AEP anion / H ₂ O		
	AEP cation, AEP anion / H ⁺ PZCOO ⁻		
	PZ cation, PZ anion / H ⁺ AEP ⁻ COO ⁻		
PZ cation, PZ anion / -OOCAEPH ⁺			

4.2 RESULTS AND DISCUSSION

4.2.1 Identification of ^{13}C NMR spectra

Quantitative ^{13}C NMR was used in this work to investigate the species distribution in AEP- H_2O - CO_2 and PZ-AEP- H_2O - CO_2 , and validate the model prediction of speciation. Due to the rapid exchange rate of protons, a protonated/di-protonated species and the unprotonated counterparts cannot be differentiated by the NMR spectroscopy used in this study. Therefore it is the sum of them that was quantified from the NMR spectra. Potential species in the PZ-AEP- H_2O - CO_2 system are listed in Table 4.1. The identification of NMR peaks in loaded 6 m AEP and 5 m PZ/2 m AEP is shown in Figure 4.1. Due to the long distance between the primary and secondary amino groups in AEP, the addition of a carboxyl group to a $-\text{NH}_2$ does not affect the chemical shift of the C on the other side. This led to the overlap of peaks from different species as shown in Figure 4.1.

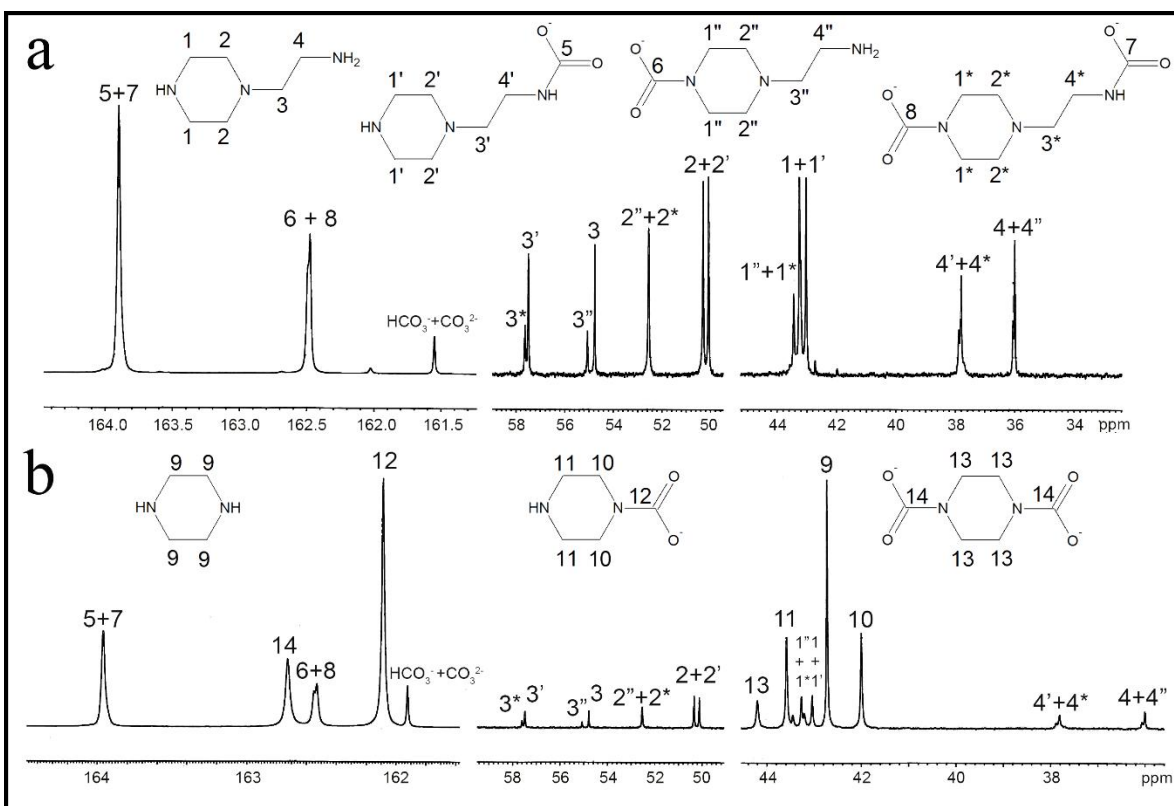


Figure 4.1: ^{13}C NMR spectra for 6 m AEP (a) and 5 m PZ/2 m AEP (b) at 25 °C and CO_2 loading of 0.3.

4.2.2 AEP- H_2O

The amine vapor pressure of 0.7 m and 5 m AEP from 40 – 70 °C has been measured in a stirred reactor coupled with a hot gas FTIR analyzer (Fourier Transform Infrared Spectroscopy, Temet Gaset Dx-4000). The details of the experimental apparatus, procedure, and analytical methods were described by Nguyen (2011). The volatility data were regressed to determine Henry's constant coefficients of AEP in water (Equation 11) and molecule-molecule binary interaction parameters τ_{mm} for the AEP/ H_2O pair (Equation 24). The regression results are given in Table 4.3. All parameters concerning AEP/ H_2O were held constant during subsequent regressions. After the regression, the model predicts the volatility of AEP well (Figure 4.2). The

volatility of AEP was found to be just 1% of the volatility of aqueous PZ with similar alkalinity and no CO₂ loading, indicating a negligible amine loss owing to volatilization, but a potential difficulty with thermal reclaiming.

Table 4.3: Regressed parameters and standard error for AEP/H₂O regression.

Parameter	Species	Value (SI units)	Standard deviation
$\tau_{mm}/1$	H ₂ O/AEP	3.3	0.19
Henry/1	AEP/H ₂ O	36	1.5
Henry/2	AEP/H ₂ O	-10780	507

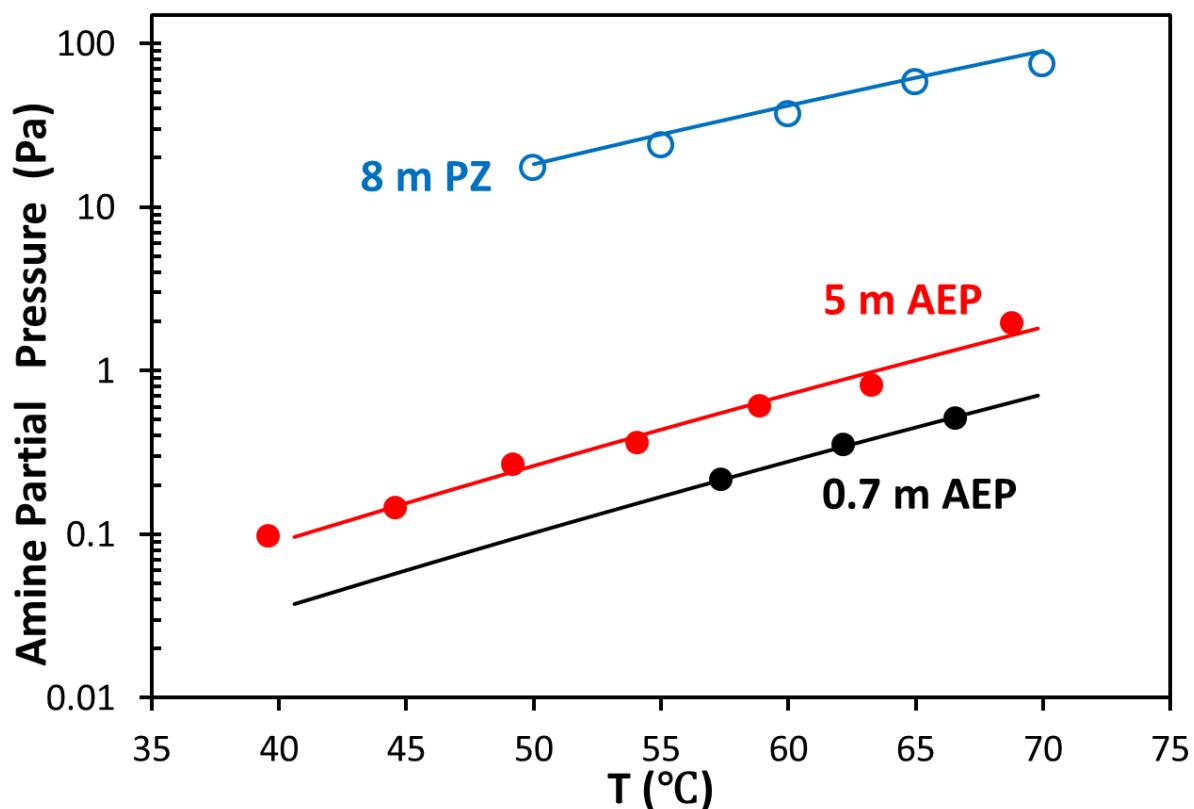


Figure 4.2: AEP vapor pressure predicted by the model compared with experimental data, as well as data for 8 m PZ with no CO₂ loading (Nguyen et al., 2011). Filled Points: Experimental data; Solid lines: Model prediction from this work.

4.2.3 AEP-H₂O-CO₂

The vapor-liquid equilibrium (VLE) of CO₂ for 6 m AEP has been measured with a wetted wall column at temperatures up to 100 °C (Chen and Rochelle 2011). These CO₂ solubility data were used for data regression. After the initial regression of the VLE data the model did not predict the speciation. As Aspen Plus® is not configured to regress speciation data, the free energy of formation of AEP carbamate species was manually adjusted to fit the NMR speciation data at 25 °C, and then standard enthalpies of formation were regressed again to get a better prediction of CO₂ solubility. This process was repeated to get a reasonable prediction for both CO₂ solubility and speciation (Figures 4.3 and 4.4). From the VLE prediction, the CO₂ cyclic capacity of this solvent is calculated as 0.71 mol/kg (AEP + water), using the following equation.

$$Capacity = \frac{(\alpha_{rich} - \alpha_{lean}) \cdot mol\ alkalinity}{kg\ (amine + H_2O)} = \frac{mol\ CO_2}{kg} \quad (27)$$

where α_{lean} and α_{rich} are defined as the CO₂ loading with P_{CO₂*} of 0.5 and 5 kPa at 40 °C. The determined parameters are given in Table 4.3.

As mentioned earlier, the original species and their protonated/di-protonated species cannot be differentiated in the NMR spectra, so they were quantified as a group in Figure 4.4. At CO₂ loading below 0.2 mol CO₂/mol alkalinity, AEPCOO⁻/H⁺AEPCOO⁻ is the dominant CO₂ sink, followed by ⁻OOCAEP/⁻OOCAEPH⁺. At CO₂ loading above 0.25 mol CO₂/mol alkalinity, the fraction of CO₂ in the form of monocarbamate decreases with CO₂ loading, due to its conversion to AEP dicarbamate and HCO₃⁻/CO₃²⁻. The fraction of AEP dicarbamate as a CO₂ sink increases with CO₂ loading and becomes dominant at CO₂ loading above 0.37 mol CO₂/mol alkalinity. Although the fraction of HCO₃⁻/CO₃²⁻ as a CO₂ sink keeps increasing with loading, it is not dominant at loading below 0.4 mol CO₂/mol alkalinity.

Figure 4.5 shows the detailed predicted speciation for 6 m AEP at 40 °C. Free AEP decreases rapidly with CO₂ loading and is almost completely depleted at $\alpha = 0.3$ mol/mol alkalinity. AEPH⁺, AEPCOO⁻, and ⁻OOCAEP are the three major products in the lean loading range. As CO₂ loading increases to $\alpha = 0.35$, the amount of AEP(H⁺)₂, H⁺AEPCOO⁻, ⁻OOCAEPH⁺, and AEP(COO⁻)₂ is more and more significant. At α above 0.35, AEP(H⁺)₂ and H⁺AEP(COO⁻)₂ are the two dominant species, followed by HCO₃⁻. (H⁺)₂AEPCOO⁻, CO₃²⁻, and free CO₂ are not significant species in the solution across the entire CO₂ loading range.

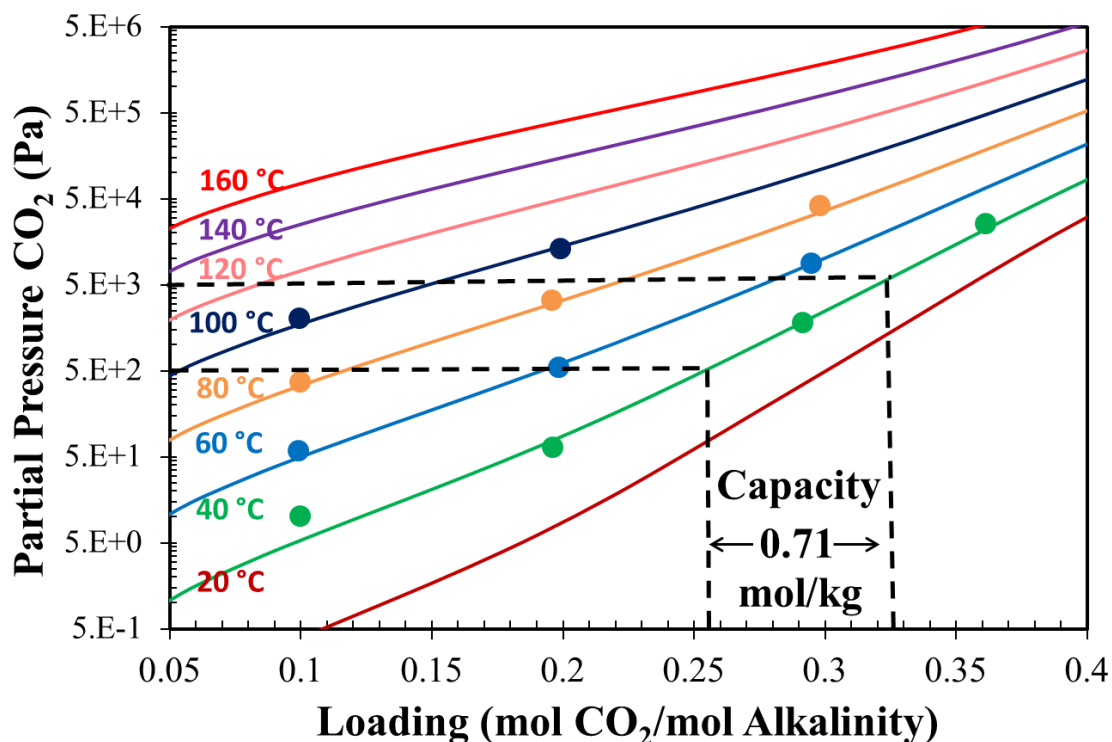


Figure 4.3: Experimental measurement (points) (Chen and Rochelle 2011) and Aspen Plus[®] predictions (lines) for VLE of loaded 6 m AEP solution between 20 °C and 160 °C

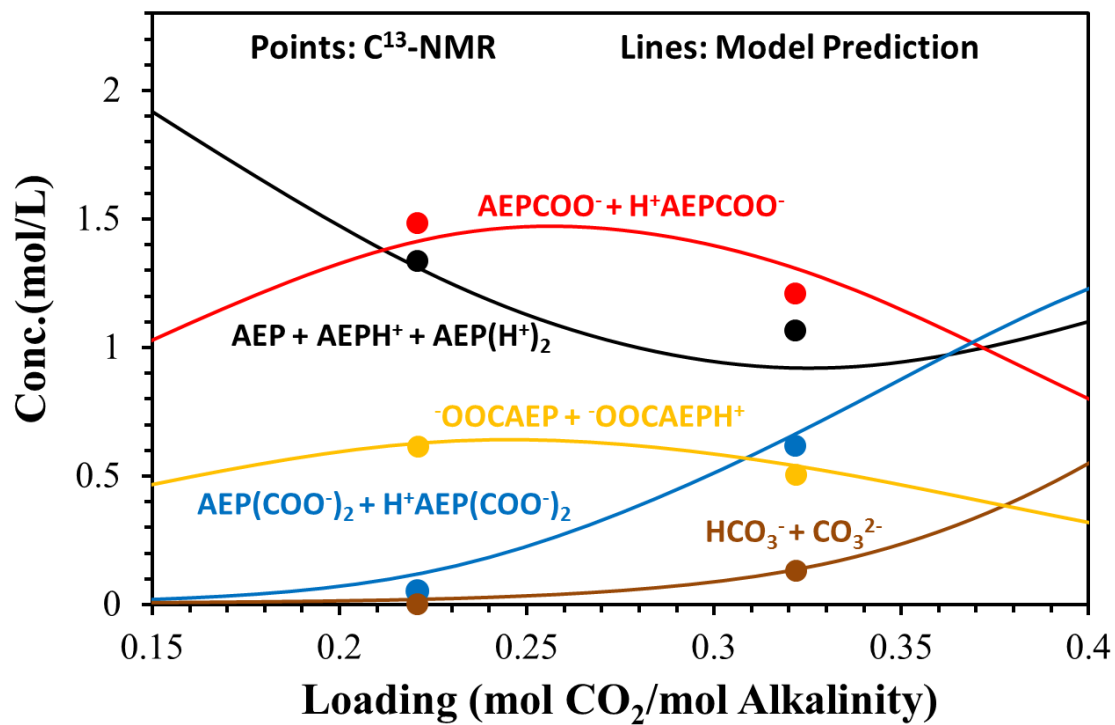


Figure 4.4: ^{13}C speciation for 6 m AEP- CO_2 - H_2O at 25 °C.

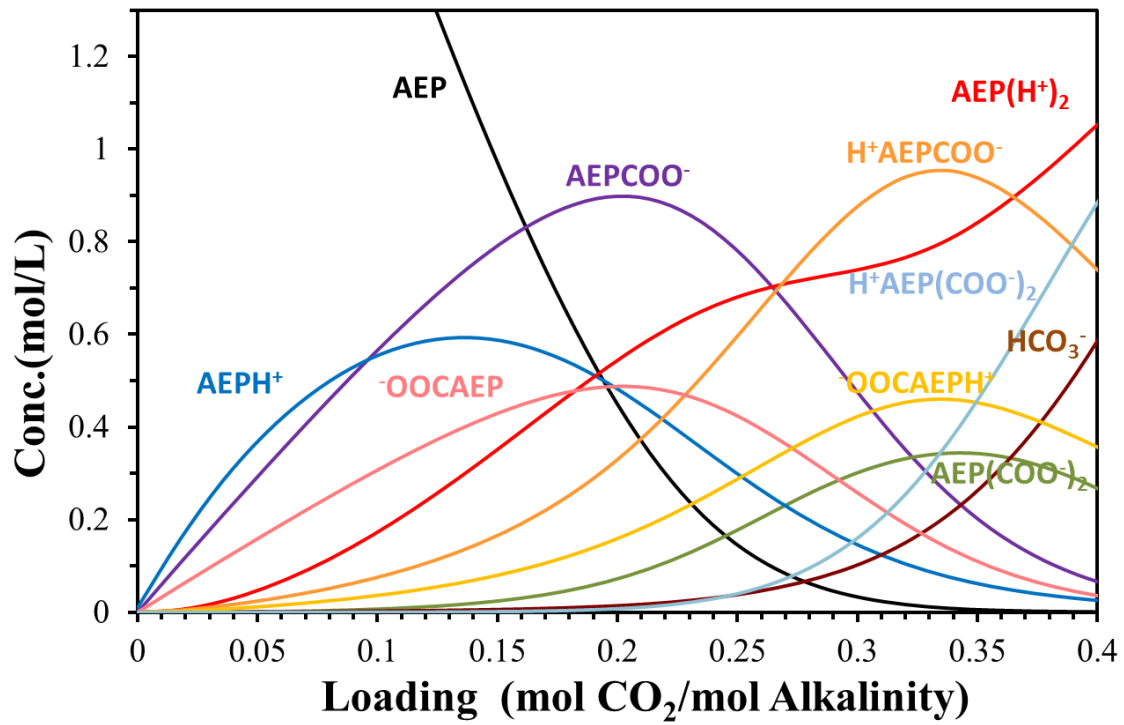


Figure 4.5: Predicted speciation distribution for 6 m AEP-CO₂-H₂O at 40 °C.

Table 4.4: The adjusted parameters for 6 m AEP-CO₂-H₂O

Parameter	Species	Value (kJ/mol)
$\Delta_f G_{i,298.15}^{\infty,aq}$	AEP ⁻ COO ⁻	-99.9
	⁻ OOCAEP	-98.0
	H ⁺ AEP(COO ⁻) ₂	-501.5
$\Delta_f G_{s,298.15}^{ig}$	H ⁺ AEP ⁻ COO ⁻	-93.5
	⁻ OOCAEPH ⁺	-91.2
$\Delta_f H_{i,298.15}^{\infty,aq}$	AEP ⁻ COO ⁻	-523.9
	⁻ OOCAEP	-515.8
	H ⁺ AEP(COO ⁻) ₂	-963.4
$\Delta_f H_{s,298.15}^{ig}$	H ⁺ AEP ⁻ COO ⁻	-550.5
	⁻ OOCAEPH ⁺	-540.1

4.2.4 PZ/AEP/H₂O/CO₂

The VLE of CO₂ for 5 m PZ/2 m AEP from 20–160 °C was regressed to determine NRTL binary interaction parameters for molecule-electrolyte pairs, $\tau_{ca,m}$, including AEP cation, PZ anion / H₂O pairs; PZ cation, AEP anion/H₂O pairs; AEP cation, AEP anion/H⁺PZCOO⁻ pairs; PZ cation, PZ anion / H⁺AEP⁻COO⁻ (Equation 25).

After regression, the VLE of CO₂ in 5 m PZ/2 m AEP is predicted well by the model (Figure 4.6), especially at the normal operating conditions of the absorber (40–60 °C and loading from 0.290–0.371). From the VLE prediction, the CO₂ cyclic capacity of this solvent is calculated as 0.78 mol/kg (PZ + AEP + water), compared to 0.50 mol/kg for 7 m MEA and 0.86 mol/kg for 8 m PZ. The higher CO₂ capacity leads to lower solvent flow rate for a specific CO₂ removal requirement, and thus less sensible heat demand for stripping. The regressed parameters are summarized in Table 4.4. The non-regressed or non-adjusted parameters used in this model are summarized in Table 4.5 (for non-temperature dependence parameters) and Table 4.6 (for non-temperature dependence parameters).

NMR measurement for 5 m PZ/2 m AEP at 25 °C was used to validate the prediction of speciation by this model. The prediction of the model is in good

agreement with the experimental NMR measurements (Figure 4.7). $\text{PZCOO}^- / \text{H}^+\text{PZCOO}^-$ is the dominant CO_2 sink in the solution across the entire CO_2 loading range, followed by $\text{AEP}^-\text{COO}^- / \text{H}^+\text{AEP}^-\text{COO}^-$. The share of PZ dicarbamate as a CO_2 sink increases with CO_2 loading and becomes significant at rich CO_2 loading. The share of $\text{OOCAEP}^- / \text{OOCAEPH}^+$ and AEP dicarbamate as a CO_2 sink is not significant across the loading range, and the share of $\text{HCO}_3^- / \text{CO}_3^{2-}$ is negligible.

Figure 4.8 shows the detailed predicted speciation for 5 m PZ/2 m AEP at 40 °C. For simplicity, species with concentration below 0.1 mol/L across the entire loading range are not shown (including AEPH^+ , AEP^-COO^- , OOCAEP^- , $\text{AEP}^-\text{(COO}^-)_2$, $\text{H}^+\text{AEP}^-\text{(COO}^-)_2$, and $(\text{H}^+)_2\text{AEP}^-\text{COO}^-$). Free PZ and AEP decreases drastically with CO_2 loading and are almost completely depleted at $\alpha = 0.35$ mol/mol alkalinity. PZH^+ and PZCOO^- are the two major products in the lean loading range and reach their maximum at $\alpha = 0.3$ and $\alpha = 0.2$ mol/mol alkalinity, respectively. As CO_2 loading increases, the amount of H^+PZCOO^- , $\text{H}^+\text{AEP}^-\text{COO}^-$, $\text{PZ}^-\text{(COO}^-)_2$, and $\text{AEP}^-\text{(H}^+)_2$ is more and more significant. HCO_3^- is not a significant species in the solution across the entire CO_2 loading range.

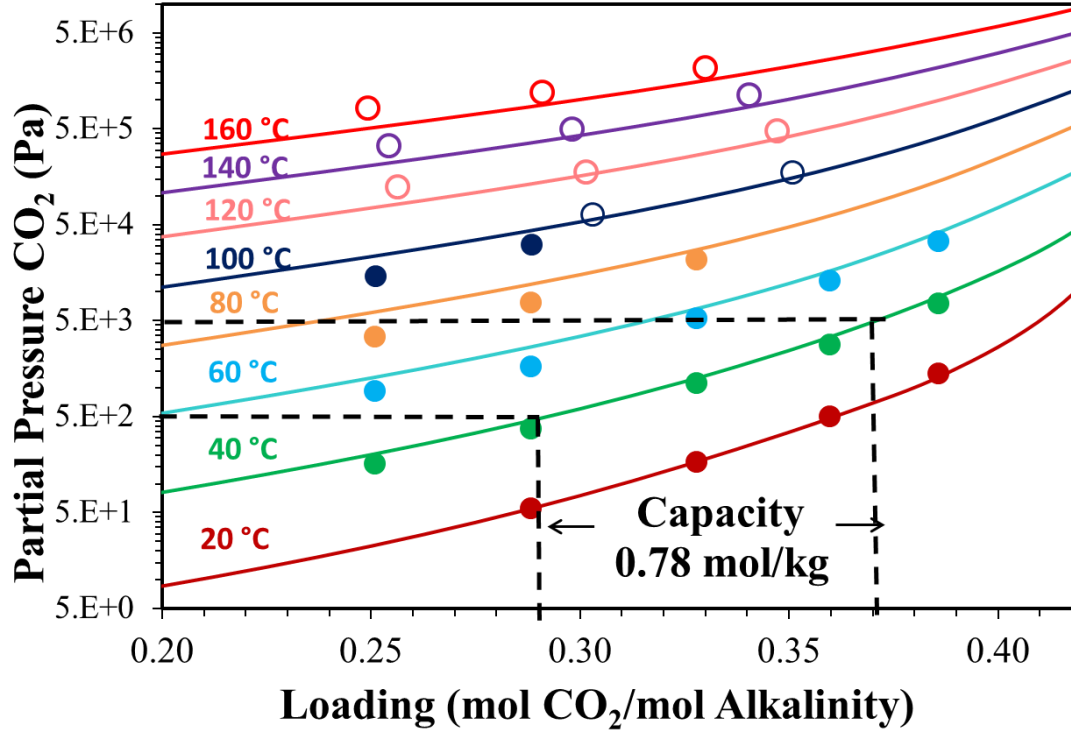


Figure 4.6: Comparison of Aspen Plus[®] predictions (lines) and experimental data (points) for loaded 5 m PZ/2 m AEP between 20 °C and 160 °C.

Table 4.5: Regressed parameters and standard error.

Parameter	Species	Value	Standard error	Default
$\tau_{ca,m}$	(PZH ⁺ , AEPCOO ⁻) H ₂ O	-6.08	25	-4
	(PZH ⁺ , OOCAEP) H ₂ O	-6.04	32	-4
	(PZH ⁺ , AEP(COO ⁻) ₂) H ₂ O	-5.20	39	-4
	(AEP(H ⁺) ₂ , PZ(COO ⁻) ₂) H ⁺ PZCOO ⁻	-7.01	9	-2

Table 4.6: Summary of non-adjusted and non-temperature dependence parameters used in this model.

Parameter	Species	Value (kJ/mol)
$\Delta_f G_{i,298.15}^{\infty,aq}$	AEPH ⁺	210.4
	AEP(H ⁺) ₂	162.2
	(H ⁺) ₂ AEP ⁻ COO ⁻	-30.4
$\Delta_f H_{i,298.15}^{\infty,aq}$	AEPH ⁺	-117.0
	AEP(H ⁺) ₂	-160.0
	(H ⁺) ₂ AEP ⁻ COO ⁻	-601.1

Table 4.7: Summary of non-adjusted and temperature dependence parameters used in this model.

Comp.	Parameters			
	a	b	c	d
	Henry's constants (bar): $\ln H_{i,s} = a_{i,s} + \frac{b_{i,s}}{T} + c_{i,s} \times \ln(T) + d_{i,s} \times T$			
H ⁺ AEP ⁻ COO ⁻ / H ₂ O	-20	0	0	0
⁻ OOCAEPH ⁺ / H ₂ O	-20	0	0	0
	Ideal gas heat capacity(J/kmol-K): $C_{p,i}^{ig} = a_i + b_i \times T + c_i \times T^2 + d_{i,s} \times T^3$			
H ⁺ AEP ⁻ COO ⁻	-54909	1289	-0.96	0.00029
⁻ OOCAEPH ⁺	-54909	1289	-0.96	0.00029
	Aqueous Infinite Dilution Heat Capacity(J/kmol-K): $C_{p,i}^{\infty,aq} = a_i + b_i \times T + c_i \times T^2 + d_{i,s} / T$			
AEPH ⁺	-40709	956	-0.71	0.00021
AEP(H ⁺) ₂	-40709	956	-0.71	0.00021
AEP ⁻ COO ⁻	-54909	1289	-0.96	0.00029
⁻ OOCAEP	-54909	1289	-0.96	0.00029
AEP(COO ⁻) ₂	-68794	1615	-1.20	0.00036
H ⁺ AEP(COO ⁻) ₂	-68794	1615	-1.20	0.00036
(H ⁺) ₂ AEP ⁻ COO ⁻	-54909	1289	-0.96	0.00029

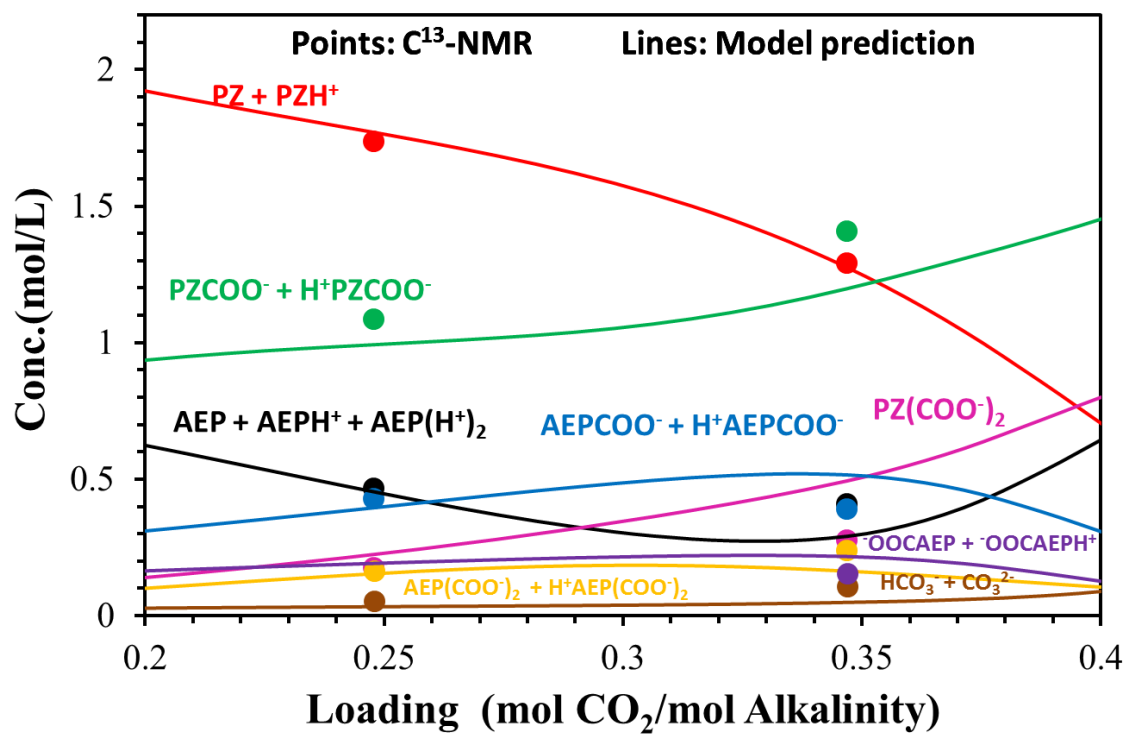


Figure 4.7: Speciation validation for 5 m PZ/2 m AEP.

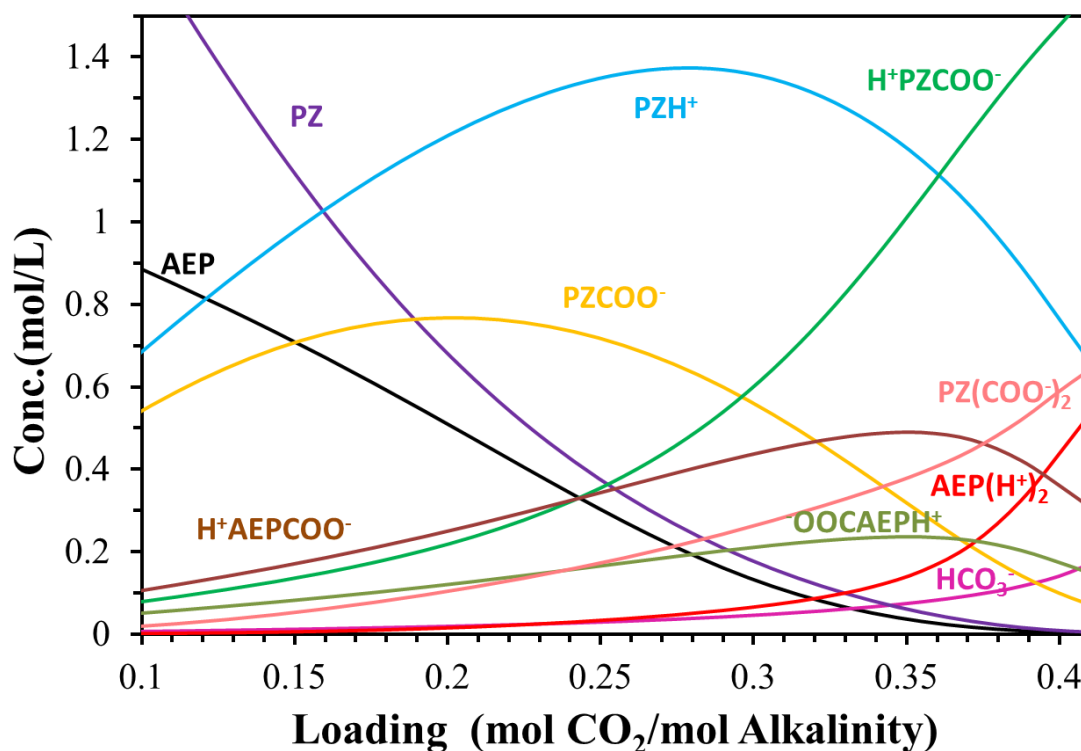


Figure 4.8: Predicted speciation distribution for 6 m AEP-CO₂-H₂O at 40 °C.

4.2.5 Heat of absorption prediction

The prediction of heat of absorption for 6 m AEP and 5 m PZ/2 m AEP is shown in Figures 4.9 and 4.10. At 40 °C the heat of absorption of 6 m AEP is 50 – 70 kJ/mol CO₂ at the operating loading range (0.255 – 0.325) and the heat of absorption of 5 m PZ/2 m AEP is 75 – 80 kJ/mol CO₂ at the operating loading range (0.290 – 0.371). The decrease of heat of absorption with loading is due to the production of HCO₃⁻ at rich loading, which gives a low enthalpy reaction between CO₂ and H₂O. Heat of absorption predictions in Aspen Plus[®] can be calculated using the calorimetric method and the Lewis and Randall equation. The use of these two methods to calculate heat of absorption has been described previously by Frailie (2011). In this model, these two methods give slightly inconsistent results of H_{abs-CO₂} at rich loading. The slight discrepancy of

prediction between these two methods is thought to be inaccuracy of the calorimetric method.

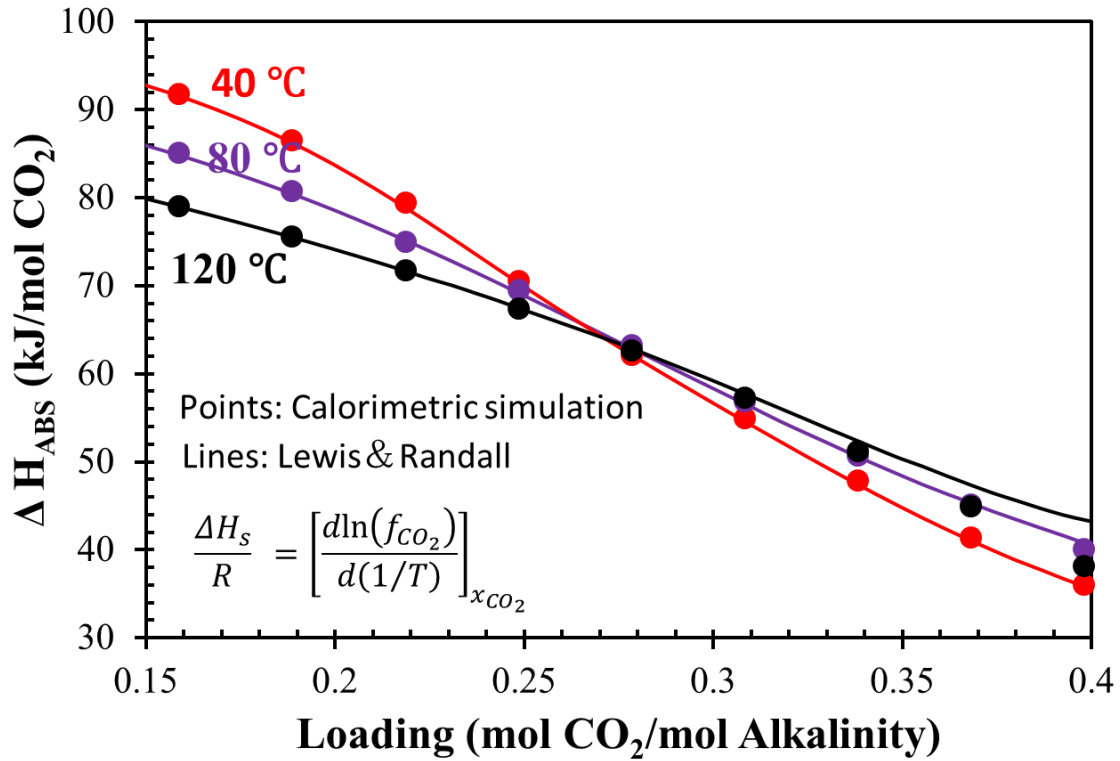


Figure 4.9: Aspen Plus[®] model predictions of heat of absorption for 6 m AEP using Lewis and Randall Equation (points) and calorimetric (lines) calculations.

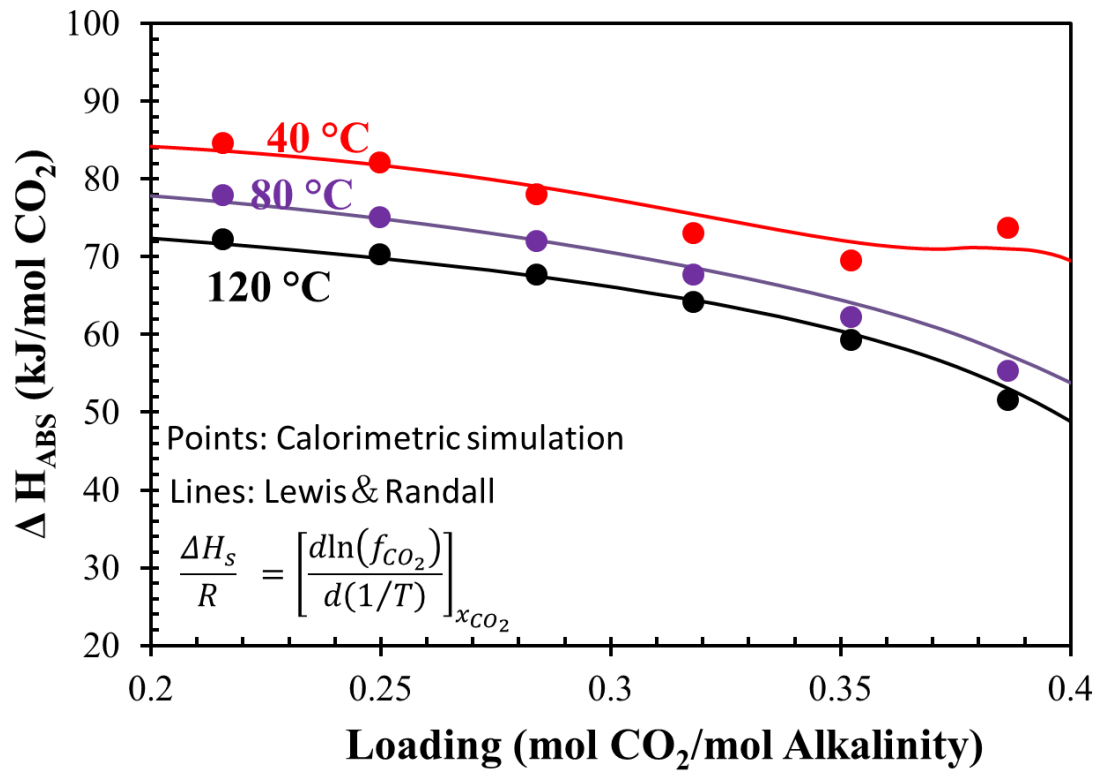


Figure 4.10: Aspen Plus® model predictions of heat of absorption for 5 m PZ/2 m AEP using Lewis and Randall Equation (points) and calorimetric (lines) calculations.

Chapter 5: Conclusions

The blend 5 m PZ/2 m AEP has a larger solid solubility window than 8 m PZ. For 5 m PZ/2 m AEP, a CO₂ loading of approximately 0.22 mol/mol alkalinity is required to maintain a liquid solution without precipitation at room temperature (20 °C), which is lower than 0.26 mol/mol alkalinity required for 8 m PZ. No precipitate was observed in PZ/AEP at rich CO₂ loading. The viscosity of 5 m PZ/2 m AEP is comparable to 8 m PZ. 5 m PZ/2 m AEP is thermally stable up to 150 °C but not 175 °C. Thermal degradation of this blend is comparable to 8 m PZ, but significantly slower than 7 m MEA. In terms of the production of total formate, the oxidation of 5 m PZ/2 m AEP is comparable to that of 8 m PZ, but significantly slower than that of 7 m MEA. The cyclic capacity of 5 m PZ/2 m AEP calculated from CO₂ solubility measurement (0.68 mole per kg amines + water) is lower than that of 8 m PZ (0.86 mole per kg amines + water), but still higher than that of 7 m MEA (0.50 mole per kg amines + water). Kinetics measurements have shown that compared to 8 m PZ, at 40 °C 5 m PZ/2 m AEP has similar CO₂ absorption rates. The formation and decomposition rate of nitrosamine in PZ/AEP is similar to that in PZ.

A thermodynamic model was developed for PZ-AEP-H₂O-CO₂ in the framework of the eNRTL model by sequential data regression. The prediction for CO₂ solubility and speciation is in good agreement with the experimental data. From the VLE prediction, the CO₂ cyclic capacity of 6 m AEP is 0.71 mol/kg (AEP + water) and the CO₂ cyclic capacity of 5 m PZ/2 m AEP is 0.78 mol/kg (PZ + AEP + water).

Speciation prediction from the model shows that in AEP-H₂O-CO₂, at lean loading, AEP⁻COO⁻ / H⁺AEP⁻COO⁻ is the dominant CO₂ sink, followed by ⁻OOCAEP / ⁻OOCAEPH⁺. The share of AEP dicarbamate as a CO₂ sink increases with CO₂ loading

and becomes dominant at rich CO₂ loading. The share of HCO₃⁻/CO₃²⁻ as a CO₂ sink is not significant at loading below 0.4 mol CO₂/mol alkalinity. For 6 m AEP, free AEP is depleted at $\alpha = 0.3$ mol/mol alkalinity. AEPH⁺, AEPCOO⁻, and ⁻OOCAEP are the three major products in the lean loading range. As CO₂ loading increases to $\alpha = 0.35$, the amount of AEP(H⁺)₂, H⁺AEPCOO⁻, ⁻OOCAEPH⁺, and AEP(COO⁻)₂ is more and more significant. At α above 0.35, AEP(H⁺)₂ and H⁺AEP(COO⁻)₂ are the two dominant species, followed by HCO₃⁻. (H⁺)₂AEPCOO⁻, CO₃²⁻, and free CO₂ are not significant species in the solution across the entire CO₂ loading range.

Heat of absorption for 6 m AEP and 5 m PZ/2 m AEP decreases with CO₂ loading, due to the production of HCO₃⁻ at rich loading. At 40 °C the heat of absorption of 6 m AEP is about 50 – 70 kJ/mol CO₂ at operation loading range (0.255 – 0.325) and the heat of absorption of 5 m PZ/2 m AEP is around 75 – 80 kJ/mol CO₂ at operation loading range (0.290–0.371).

In conclusion, compared to 8 m PZ, 5 m PZ/2 m AEP has greater solvent solubility, higher heat of CO₂ absorption, and comparable CO₂ absorption rate, solvent loss rate and potential environmental impact from nitrosamine formation, indicating that 5 m PZ/2 m AEP is a promising solvent for CO₂ capture by absorption/stripping.

Appendix A: Tabulated Experimental Data

Table A. 1: Transition temperatures for PZ/AEP blend

PZ/AEP (m)	CO ₂ (mol/mol alk)	Crystal T (°C)	Melting T (°C)
5/2	0	38.0	40.0
5/2	0.05	36.5	37.0
5/2	0.10	33.0	34.0
5/2	0.15	26.5	31.0
5/2	0.20	19.0	21.5
5/2	0.23	18.0	19.0
5/2	0.25	2.5	4
5/2	0.30	≤0	—
4/2.67	0	35.5	36.5
4/2.67	0.05	32.0	33.0
4/2.67	0.10	28.5	31.0
4/2.67	0.15	24.0	25.0
4/2.67	0.20	17.5	20.0
4/2.67	0.23	8.0	12.0
4/2.67	0.25	≤0	—
3/3.33	0	33.0	34.0
3/3.33	0.05	27.0	31.0
3/3.33	0.10	24.0	25.0
3/3.33	0.15	18.0	19.0
3/(3.33)	0.20	16.0	16.0
3/3.33	0.23	2.5	4.0
3/3.33	0.25	≤0	—

—: not measured

Table A. 2: Tabulated Experimental Data for thermal degradation of 5 m PZ/2 m AEP (0.3 mole CO₂ per mole alkalinity initially, 175 °)

Time (Days)	PZ	AEP	NH ₄ ⁺	PEP	AEAEPZ (T)	EPZ + TEDA	DAEP	Formate (T)	CO ₂
	concentration (mmol/kg solvent)								
0	2502.1	1015.5	0.0	0.0	0.0	0.0	0.0	2.5	2759.8
1	2497.7	929.5	0.0	38.5	32.4	0.0	0.0	16.9	2543.1
2	2394.0	850.9	48.2	42.6	37.2	0.0	0.0	68.5	2418.2
3	2178.6	771.9	69.7	47.9	69.4	0.0	0.0	129.9	2388.9
4	2074.9	678.1	60.8	45.3	64.4	0.0	0.0	145.3	2408.3
5	2022.8	707.2	105.1	55.8	80.3	0.0	0.0	209.7	2311.7
14	1855.7	555.9	181.2	61.2	86.9	0.0	0.0	311.8	2142.4
21	1808.3	612.8	261.6	70.3	113.9	26.8	34.9	439.7	2075.0
29	1664.2	434.1	326.4	70.6	97.2	30.9	35.8	439.3	1950.0
35	1514.1	370.9	312.3	68.7	94.2	31.5	35.3	466.6	1830.5
70	1037.2	227.6	455.1	61.6	61.2	62.7	35.7	573.6	1389.9
105	585.6	130.8	587.0	55.0	62.0	73.3	38.8	585.3	1079.4
140	536.0	99.8	690.0	52.3	57.7	76.8	40.2	579.3	999.1

Table A. 3: Tabulated Experimental Data for oxidation of 2 m AEP at 70 °C in the presence of 0.1 mM Mn²⁺ and with the typical SSM mixture (0.4 mM Fe²⁺, 0.05 mM Cr³⁺ and 0.1 mM Ni²⁺)

Time (Days)	AEP	Acetate	Formate	Total Formate	Oxalate	Sulfate	PZ
	m	concentration (mmol/kg solvent)					
0.00	1.90	0.00	0.00	0.00	0.00	2.04	0.00
0.25	1.84	3.12	1.31	1.22	0.28	2.04	0.00
0.97	1.81	3.11	2.11	1.96	0.27	1.98	2.46
1.33	1.80	3.20	2.71	2.35	0.27	1.99	2.33
3.02	1.84	3.08	5.13	4.85	0.26	1.98	11.75
3.24	1.81	2.97	5.04	5.25	0.23	1.99	12.48
5.29	1.76	2.89	6.91	9.25	0.25	1.96	18.13
7.27	1.79	2.95	9.76	13.71	0.25	1.96	25.86
9.31	1.60	2.62	11.59	17.73	0.23	1.95	26.77
13.06	1.62	2.70	18.80	30.02	0.22	1.95	40.47

Table A. 4: Tabulated Experimental Data for oxidation of 8 m PZ at 70 °C in the presence of 0.1 mM Mn²⁺ and with the typical SSM mixture (0.4 mM Fe²⁺, 0.05 mM Cr³⁺ and 0.1 mM Ni²⁺)

Time (Days)	PZ	Acetate	Formate	Total Formate	Oxalate	Sulfate
	m	concentration (mmol/kg solvent)				
0.00	8.00	0.00	0.00	0.00	0.00	2.00
0.25	8.00	0.00	0.17	0.31	0.29	2.00
1.33	7.93	0.00	0.27	0.50	0.24	1.83
3.02	8.01	0.09	0.28	0.89	0.18	1.59
3.24	8.44	0.12	0.34	1.07	0.20	1.77
5.29	8.55	0.14	0.52	2.16	0.20	1.84
7.27	8.19	0.15	0.80	3.66	0.21	1.94
9.31	7.72	0.17	1.05	5.38	0.22	2.11
13.06	8.70	0.20	1.64	8.93	0.17	1.83

Table A. 5: Tabulated Experimental Data for formation of nitrosamines in 5 m PZ/2 m AEP and 2 m AEP at 0.3 mol CO₂/mol alkalinity and 100 °C

Time (Hours)	MNPZ in 5 m PZ/2 m AEP	MNAEP in 5 m PZ/2 m AEP	MNAEP in 2 m AEP
	concentration (mmol/kg solvent)		
0.00	0.00	0.00	0.00
3.25	0.51	0.09	0.48
5.20	0.62	0.11	0.64
7.17	0.68	0.14	0.76
8.60	0.69	0.17	0.82

Table A. 6: Tabulated Experimental Data for nitrosamine decomposition in 5 m PZ/2 m AEP and 2 m AEP at 0.3 mol CO₂/mol alkalinity and 150 °C

Time (Days)	MNPZ in 5 PZ/2 AEP	MNAEP in 5 PZ/2 AEP	MNAEP in 2 AEP
	concentration (mmol/kg solvent)		
0.03	27.75	6.82	14.27
0.13	23.55	5.89	28.88
0.25	15.36	4.02	25.67
0.51	6.67	1.83	19.53
1.03	1.81	0.59	13.70
2.04	0.00	0.00	6.55
3.10	0.00	0.00	3.71
4.02	0.00	0.00	1.47

Table A. 7: Tabulated Experimental Data for CO₂ solubility in 5 m PZ/2 m AEP at high temperature

T (°C)	CO ₂ (mol/mol alk)	P _{CO2}
100	0.303	64737
100	0.351	176702
110	0.349	303304
120	0.257	121862
120	0.302	173700
120	0.347	471571
130	0.256	207569
130	0.300	295133
130	0.344	753328
140	0.254	325105
140	0.298	489246
140	0.341	1110000
150	0.253	503152
150	0.295	774416
150	0.336	1552360
160	0.249	805699
160	0.291	1180000
160	0.330	2150000

References

- Austgen, D. M., Rochelle, G. T., et al. (1989). Model of vapor-liquid equilibria for aqueous acid gas-alkanolamine systems using the electrolyte-NRTL equation. *Ind Eng Chem Res.* 28(7): 1060-1073.
- Chen, C.-C., Bokis, C. P., et al. (2001). Segment-based excess Gibbs energy model for aqueous organic electrolytes. *AIChE Journal.* 47(11): 2593-2602.
- Chen, X. and Rochelle, G. T. (2011). Aqueous piperazine derivatives for CO₂ capture: Accurate screening by a wetted wall column. *Chem Eng Res Des.* 89(9): 1693-1710.
- Fine, N. A., Goldman, M. J., et al. (2013). Managing n-nitrosopiperazine and dinitrosopiperazine. *Energy Procedia.* 37(0): 273-284.
- Frailie, P., Plaza, J., et al. (2011). Modeling piperazine thermodynamics. *10th International Conference on Greenhouse Gas Control Technologies.* 4: 35-42.
- Freeman, S. A. (2011). Thermal Degradation and Oxidation of Aqueous Piperazine for Carbon Dioxide Capture, The University of Texas at Austin.
- Freeman, S. A., Dugas, R., et al. (2009). Carbon dioxide capture with concentrated, aqueous piperazine. *Energy Proced.* 1(1): 1489-1496.
- Freeman, S. A. and Rochelle, G. T. (2011). Thermal degradation of piperazine and its structural analogs. *10th International Conference on Greenhouse Gas Control Technologies.* 4: 43-50.
- Hilliard, M. D. (2008). A Predictive Thermodynamic Model for an Aqueous Blend of Potassium Carbonate, Piperazine, and Monoethanolamine for Carbon Dioxide Capture from Flue Gas. Austin, The University of Texas at Austin.
- Li, L., Li, H., et al. (2013). Absorption rates and CO₂ solubility in new piperazine blends. *Energy Procedia.* 37(0): 370-385.
- Li, L., Voice, A. K., et al. (2013). Amine blends using concentrated piperazine. *Energy Procedia.* 37(0): 353-369.
- Nguyen, T., Hilliard, M., et al. (2011). Volatility of aqueous amines in CO₂ capture. *Energy Procedia.* 4(0): 1624-1630.
- Pagano, J. M., Goldberg, D. E., et al. (1961). A thermodynamic study of homopiperazine, piperazine and n-(2-aminoethyl)-piperazine and their complexes with copper(ii) ion. *The Journal of Physical Chemistry.* 65(6): 1062-1064.
- Posey, M. L. and Rochelle, G. T. (1997). A Thermodynamic Model of Methyl-diethanolamine-CO₂-H₂S-Water. *Ind Eng Chem Res.* 36(9): 3944-3953.

- Rochelle, G., Chen, E., et al. (2011). Aqueous piperazine as the new standard for CO₂ capture technology. *Chem Eng J.* 171(3): 725-733.
- Rochelle, G. T. (2009). Amine scrubbing for CO₂ capture. *Science.* 325(5948): 1652-1654.
- Sexton, A. J. and Rochelle, G. T. (2009). Catalysts and inhibitors for oxidative degradation of monoethanolamine. *Int J Greenh Gas Con.* 3(6): 704-711.
- Xu, Q. (2011). Thermodynamics of CO₂ Loaded Aqueous Amines. Austin, The University of Texas at Austin.